Submitted to
J. Chem. Phys.

LBL-1886
Preprint

c. 1

DYNAMICS OF THE O^+-H_2 REACTION. II: REACTIVE AND NONREACTIVE SCATTERING OF $O^+(^4S_{3/2})$ AT RELATIVE ENERGIES ABOVE 13 eV

Keith T. Gillen, Bruce H. Mahan, and John S. Winn

September 1973

Prepared for the U. S. Atomic Energy Commission
under Contract W-7405-ENG-48

For Reference

Not to be taken from this room

LAWRENCE BERKELEY LABORATORY
UNIVERSITY OF CALIFORNIA
BERKELEY

LBL-1886

DISCLAIMER

This document was prepared as an account of work sponsored by the United States Government. While this document is believed to contain correct information, neither the United States Government nor any agency thereof, nor the Regents of the University of California, nor any of their employees, makes any warranty, express or implied, or assumes any legal responsibility for the accuracy, completeness, or usefulness of any information, apparatus, product, or process disclosed, or represents that its use would not infringe privately owned rights. Reference herein to any specific commercial product, process, or service by its trade name, trademark, manufacturer, or otherwise, does not necessarily constitute or imply its endorsement, recommendation, or favoring by the United States Government or any agency thereof, or the Regents of the University of California. The views and opinions of authors expressed herein do not necessarily state or reflect those of the United States Government or any agency thereof or the Regents of the University of California.

LBL 1886

Dynamics of the O^+-H_2 Reaction. II: Reactive and Nonreactive Scattering of $O^+(^4S_{3/2})$ at Relative Energies above 13 eV

Keith T. Gillen, Bruce H. Mahan, and John S. Winn
Department of Chemistry, and Inorganic Materials Research Division of the Lawrence Berkeley Laboratory, University of California, Berkeley, California

Abstract

We report velocity vector distributions for the reactive and nonreactive scattering of O^+ by H_2, D_2, and HD in the relative energy range 13 - 50 eV. Essentially no very small angle reactive scattering is observed for any of these systems. In the lower and intermediate parts of the energy range, the product of the $O^+(D_2,D)OD^+$ reaction reaches a maximum intensity near 50°, and decreases somewhat at larger angles. This shape is maintained but with decreasing intensity from 15 - 30 eV relative energy. At higher energies, the distribution moves to larger angles and the intensity continues to drop. From 13 to 20 eV, OH^+ from O^+-HD collisions peaks near 35°, and has little intensity at larger angles, while the corresponding OD^+ product rises to a broad maximum near 90°, and is only slightly less intense at larger angles. At relative energies above

13 eV the nonreactive scattering of O^+ has a major component that corresponds to the elastic impulsive scattering of O^+ from <u>one</u> atom of the target. Nonreactive scattering from HD shows two peaks which correspond to impulsive O^+-H or O^+-D collisions. The experimental results are compared to the predictions of a model in which reaction occurs as the result of those sequences of two-body hard sphere interactions which lead to bound product molecules. The general forms of the product angular distributions and their dependence on the isotopic composition of the target are fairly well represented by the model. For other features such as the experimental energy dependence of the total cross section ($\sigma \propto E_{rel}^{-7/2}$) and the corresponding isotope effect, the model is less successful. A convenient velocity vector diagram method is given which allows a simple, edifying analysis of product angular distributions to be made with a compass and straightedge.

One of the major goals of the study of molecular dynamics is to develop models which allow the interpretation of the important features of reaction phenomena and provide the tools by which predictions of the behavior of experimentally untried systems can be made. As alternatives to the expensive numerical calculation of exact trajectories on a complete potential energy surface, a number[1-9] of simple models for the reaction process have been proposed. Even allowing for the necessity of using extremely simple approximations to the potential energy surface, most of these models are to a greater or lesser degree lacking in generality and rigor.

One of the models which is most attractive from the point of view of conceptual simplicity and capacity for refinement is the sequential impulse model of Bates, Cook, and Smith.[1] In brief, the reaction A(BC,C)AB is viewed as an event in which A hits B impulsively, B hits C in a like manner, and A combines with B (or C) if the appropriate energy of relative motion is less than the dissociation energy of the product molecule. This model has been elaborated and greatly extended by Suplinskas,[3] and George and Suplinskas,[7,8] and has proved capable of reproducing the major features of the Ar^+-D_2 reactive and non-reactive scattering. Recently, a very similar model[10] has been applied to hot atom reactions.

In the course of our investigations[11] of the reaction

$$O^+(^4S_{3/2}) + H_2 \rightarrow OH^+(^3\Sigma^-) + H \qquad (1)$$

and its isotopic variants, it became clear that some of the results might be explained qualitatively by a sequential impulse model. Since the impulse model should be most applicable to relatively high energy collision phenomena, we made a particular effort to examine[12] the reaction in the high energy regime. In this paper we report the results of our investigations of the reactive and non-reactive scattering of O^+ by H_2, D_2, and HD at relative energies in the range of 13 to 50 eV and compare the results to the predictions of a rigorous hard sphere sequential impulse model.

Experimental

The experiments are performed by allowing a collimated, energy selected beam of O^+ ions to impinge on a target gas contained in a scattering cell. The scattered ions pass through an electrostatic energy analyzer and a quadrupole mass filter before being detected by an ion counter. The detector components and exit aperture of the scattering cell are mounted on a rotatable lid, which permits the intensity of scattered ions to be measured at various angles and energies. The preparation and characterization of the O^+ beam was described in our previous publication.[11] At least 97% of the oxygen ions in the momentum analyzed beam were in their $^4S_{3/2}$ ground state.

Our experimental results are presented principally in the form of contour maps of the specific intensity $\bar{I}(\theta,u)$,

the intensity of ions per unit velocity space volume normalized to unit beam strength, scattering gas density, and collision volume. A polar coordinate system is used with the radial coordinate u representing the speed of the ion relative to the velocity of the center-of-mass of the complete target-projectile system, and the angular coordinate θ measured with respect to the original direction of the projectile ion beam. The specific intensity is normalized such that

$$\bar{\sigma} = 2\pi \int_0^{\pi} \sin\theta \, d\theta \int_0^{\infty} u^2 \, \bar{I}(\theta, u) \, du$$

is always proportional to the true total cross section σ.

Results

Before presenting the results of our experiments in the high energy regime, it is useful to summarize the behavior of the system[11,13] at relative energies below 15 eV. The reaction $O^+(H_2,H)OH^+$ is only slightly exoergic ($\Delta E_0{}^{\circ} = -0.43$ eV) when the reactants and products are in their ground states. Because one of the products is an atom whose first excitation energy is large (10 eV), certain significant limits can be placed on Q, the difference between the final and initial relative kinetic energies. Q is also given by

$$Q = -\Delta E_0{}^{\circ} - U'$$

where U' is the internal (vibrational and rotational) energy of OH^+, and $\Delta E_0{}^{\circ}$ is the standard energy change for

the reaction. Since U' is equal to or greater than zero and less than $D_o(OH^+)$, the dissociation energy of OH^+ to $O(^3P)$ and H^+, we have

$$- \Delta E_o^o - D_o \leqslant Q \leqslant - \Delta E_o^o$$

$$- 4.5 \leqslant Q < 0.43 \text{ eV}$$

for formation of OH^+ in its ground electronic state. While most OH^+ is formed in its electronic ground state, we have evidence[11] that in some collisions, the first excited state, $OH^+(^1\Delta)$, is formed. For this state, the limits on Q are

$$- 6.5 \leqslant Q \leqslant - 1.7 \text{ eV}$$

At low initial relative energies, the OH^+ product velocity vector distributions in the barycentric system are very anisotropic,[11,13] and have strong maxima at the spectator stripping velocity. The large angle scattering is of much lower intensity, but appears at all angles to lie close to the Q value which at small angles is associated with spectator stripping, and is given by

$$Q_{SS} = - \frac{B}{A + B} E_L$$

where A and B are the masses of the projectile and abstracted atom respectively, and E_L is the laboratory energy of the projectile. This behavior is maintained as the projectile energy is raised, until Q_{SS} becomes more negative than the lower limit set by the product stability requirement. At this critical projectile energy, the stripping peak is

abruptly lost, and the larger angle scattering moves to larger values of Q, where the products are stable to dissociation. The evidence[11] for formation of $OH^+(^1\Delta)$ consists of the persistence of product intensity in the range $-6.5 \leq Q < -4.5$ eV, where $OH^+(^1\Delta)$ is stable, but $OH^+(^3\Sigma^-)$ is not. Rather spectacular differences between the OH^+ and OD^+ distributions from O^+ - HD collisions occur at projectile energies which allow formation of OH^+ but not OD^+ by spectator stripping.

We can now turn to the results of the present investigation. Figure 1 shows the distribution of OD^+ obtained from the O^+ - D_2 reaction with an initial relative energy of 20.0 eV. Aside from its diminished intensity, this distribution very closely resembles the map obtained[11] in an experiment at 15 eV initial relative energy. The spectator stripping velocity, marked by a small cross in Fig. 1, lies well within the velocity region which is forbidden by product stability considerations. There is no product intensity near 0°, which indicates that the potential surface for this system does not have a feature which would allow products formed by grazing collisions to recoil directly forward into the velocity region where products are stable. The interactions between the incipient OD^+ molecule and the freed D atom which do lead to product stability also produce a deflection of the OD^+ from the original direction of the projectile. Collisions in which

this interaction is weak occur with highest frequency, lead to product scattered through moderate angles, and are probably responsible for the intensity maxima near 50° in Fig. 1. Collisions in which the impact parameter is smaller and the target orientation more nearly collinear with the projectile trajectory lead to product formation at larger angles, and are generally somewhat more efficient in stabilizing the product. Such collisions occur with lesser frequency, however, and this qualitatively accounts for the diminished intensity at larger angles which is evident in Fig. 1.

Figure 2 shows the product distribution obtained when the initial relative energy was 32.0 eV. The general shape of the distribution is similar to that obtained at 20.0 eV, but there are some differences of detail. The overall product intensity has dropped considerably, and while there is substantial scattering in the region near 50°, the maximum product intensity occurs in the region near 180°. Both these changes are consistent with the idea that as the initial relative kinetic energy is increased, giving more internal energy to the incipient OD^+, formation of a stable OD^+ product becomes more difficult. Therefore, the large angle scattering in which the interaction of the incipient OD^+ product with the freed D atom is stronger becomes relatively more important.

It is evident that much of the intensity in Fig. 2 lies outside the rather narrow band of allowed values of Q. This occurs to a greater degree as the initial relative energy is raised, because at the higher energies, the effective bandpass of our apparatus becomes larger than the velocity interval in which the products are stable. Consequently, the product speed distributions progressively become less meaningful for these higher energy experiments. Nevertheless, useful information can be derived from the product angular distributions alone.

Figure 3 shows the OD^+ intensity distribution obtained from an experiment in which the initial relative energy was 38.1 eV. The angular distribution reaches a broad maximum at 180°, with only very small intensity at angles less than 90°. Thus there has occurred a complete evolution of the product distribution from being strongly forward peaked at low energy[11,13] to backward peaked at very high energy.

In Fig. 4 we show the product distribution from an experiment in which the initial relative energy was 50 eV. The product is now exclusively in the large angle region, but the intensity peak at 180° has disappeared. The total product intensity is very low, only 10^{-3} of the total intensity from 10 eV collisions. It appears reasonable to regard 50 eV as a rough upper limit to the range of energies in which chemically significant amounts of OD^+

product are formed. If we include the rate constant measured[14] at 300°K and the low energy velocity spectra of Harris and Leventhal[13] together with our investigations,[11,12] the reaction $O^+(H_2,H)OH^+$ and its isotopic variants have been studied over a range in which the energy varies 1000-fold. It is doubtful that this can be said of any other chemical reaction.

Figures 5 and 6 show, respectively, the distribution of OH^+ and OD^+ from O^+ - HD collisions at a relative energy of 15.8 eV. There are very significant differences between these two distributions, and both differ from the distribution of OD^+ from O^+ - D_2 collisions at the same laboratory energy of the projectile (Fig. 1). In Fig. 5, we find that the OH^+ intensity reaches a maximum near 35°, and diminishes very rapidly at larger angles. Near 180°, the intensity is approximately 0.05 times the intensity at the small angle peak, whereas in the O^+ - D_2 experiment of Fig. 1, the peak intensity at large angles is only slightly less than one half the value at the small angle maximum. In Fig. 6 we see that the distribution of OD^+ from 15.8 eV O^+ - HD collisions differs dramatically from the OH^+ distribution. The OD^+ distribution reaches a broad maximum near 90°, and diminishes only slightly at larger angles. The tendency of the OH^+ product to lie at small angles while the OD^+ appeared principally at large angles was also observed in our experiments at 11.8 eV relative energy,[11] and a similar

effect was evident in experiments with the O_2^+ - HD system.[15]

Figures 7 and 8 show the OH^+ and OD^+ distributions that result from O^+ - HD collisions at 19.7 eV relative energy. They closely resemble the corresponding distributions in Figs. 5 and 6, with the major features accentuated. The OH^+ distribution again peaks in the vicinity of 35°, and falls to less than one tenth its maximum value before 90° has been reached. The OD^+ again is completely absent from the small angle region, reaches a broad maximum near 90°, and diminishes to approximately one half its maximum intensity at 180°. Compared with the distribution of OD^+ obtained from O^+ - D_2 collisions at the same relative energy (Fig. 1) the distribution of OD^+ in Fig. 8 is quite noticeably shifted to large angles.

Although we do not show the results here, the reaction of O^+ with H_2 was investigated at 13.9 and 27.8 eV. The distributions of OH^+ obtained from these experiments very much resemble the OD^+ distributions obtained from the O^+ - D_2 reaction at comparable relative energies. The major discernible difference is that near 180°, the OH^+ distributions tend to be somewhat less intense relative to the small angle (50°) maxima than is the case for the OD^+ distributions. In comparing the maps for all isotopic combinations, the most striking revelation is that the distribution of a given isotopic product depends most sensitively on the <u>ratio</u> of the mass of the freed atom to the mass of the abstracted atom.

The experimental total cross sections for reaction were determined at each energy for the various isotopic targets by integration of the specific intensity distributions over speed and angle. Although we can not assign absolute values to these total cross sections, we feel that the relative values are quite reliable. A plot of log σ vs. E_{rel} is linear over the relative energy range 8 - 50 eV, and has a slope of - 7/2. Thus the reaction cross section varies as $E_{rel}^{-7/2}$ for all isotopic targets over this energy range.

In previous investigations,[16,17] we have found that the study of the non-reactive scattering provided very useful insights into the general nature of the potential energy surface and reaction mechanism. We have found this to be particularly true in the present system. Figure 9 shows the distribution of O^+ scattered from D_2 at an initial relative energy of 20.1 eV. At angles of 45° and smaller, there is a well-defined ridge of intensity which closely follows the circle labeled $Q = 0$. This elastic component of the non-reactive scattering comes from collisions in which the O^+ makes a grazing encounter with the D_2 molecule as a whole. At these high relative energies, however, a grazing collision implies an impact parameter as small as approximately 1 Å, and a (repulsive) potential energy at the distance of closest approach of as much as 5 eV.

At angles larger than 45°, the scattering abruptly becomes very inelastic. Virtually all the intensity at large angles lies well within the circle marked Q = - 4.5 eV, which is the locus of scattering sufficiently inelastic to dissociate D_2. At 180°, the maximum O^+ intensity lies close to the circle labeled Q = - 19 eV, which corresponds to virtually the full relative energy being converted into internal motion of D_2.

A clear picture of the inelastic scattering process emerges when it is recognized that the inelastic ridge nearly follows the circle labeled "Elastic $O^+(D,D)O^+$" in Fig. 9. This circle has its origin at the velocity of the center-of-mass of O^+ and <u>one</u> D atom, and its radius is the speed of the O^+ relative to <u>this</u> center-of-mass. Thus it is the locus of elastic scattering of O^+ by a <u>free</u> D atom. The fact that the ridge of inelastically scattered O^+ nearly falls on this circle suggests that in many collisions, the O^+ interacts nearly impulsively[12] with one atom of the D_2 molecule.

Figure 10 shows that this elastic impulse picture of the inelastic scattering is even a more accurate description at the higher relative energy of 35.0 eV. The maximum of the ridge of inelastically scattered O^+ is close to the locus of elastic scattering from one D atom, which in Fig. 10 is the circle labeled V_{KO}. Thus the most probable inelastic process results from impulsive or knock-out (KO) scattering of one

of the target atoms by O^+. However, the width of the inelastic ridge in Fig. 10 is significantly greater than would be expected from purely impulsive scattering. This can be seen here and in Fig. 9 most simply by comparing the width of the inelastic ridge to the width of the elastic ridge at small angles. The broadening of the inelastic ridge is an indication that in many of the collisions, the third atom is not merely a spectator, but is subjected to a force even as the O^+ projectile interacts briefly with its target atom.

In Fig. 11, it is clear that at 50 eV relative energy, inelastic scattering again closely follows the impulse or knockout circle. The inelastic component is indeed the dominant feature of the distribution, and exceeds the integrated intensity of the small angle elastic scattering. The small crosses in the large angle region of Fig. 11 locate the maxima of a subsidiary ridge due to a new inelastic feature which will be discussed subsequently.

If the non-reactive scattering in this system is truly of an impulsive nature, the distribution of O^+ scattered by HD should ideally show two inelastic ridges, one corresponding to O^+ - H collisions, the other to O^+ - D collisions. Figure 12 shows the distribution of O^+ by HD at an initial relative energy of 27.6 eV. The loci of the impulsive scattering of O^+ by H and by D are indicated by the circles labeled $V_{KO}(H)$ and $V_{KO}(D)$ respectively. The

observed inelastic scattering in this case is a very broad ridge which covers both circles over most of the angular range. However, in the region near the center-of-mass origin, the inelastic feature does separate into two ridges. Thus the distribution of Fig. 12 is qualitatively consistent with the expectations based on the impulse model for inelastic scattering.

For reasons of clarity, the maps of scattered intensity have a limited number of contours. Consequently, some of the detail available in the experimental data is lost. It is beneficial, therefore, to examine velocity spectra, which are profiles of the product intensity measured at a laboratory angle of 0°, or along the 0° - 180° axis in the barycentric system. Figure 13 shows several such velocity spectra obtained by scattering O^+ from D_2, HD, and in one case, He. The velocities of the projectile beam, the center-of-mass, and of O^+ scattered elastically from one atom and from the total target mass are indicated. The velocity scale in each panel has been adjusted so that corresponding reference velocities fall at the same places in all spectra. The intensities are normalized to unity at the highest point measured in each spectrum.

Panels a - c show how the non-reactive scattering of O^+ by D_2 evolves as the initial relative energy increases from 13 to 49.9 eV. Even at the lowest energy shown the inelastic peak falls very near to the velocity expected

from the impulsive interaction of O^+ with one D atom. As the initial relative energy increases, the inelastic peak first falls at the impulsive knockout velocity, and then moves to a slightly higher velocity which corresponds to a collision which is nearly completely inelastic ($Q = - E_{rel}$). Concomitantly, the new inelastic feature mentioned in connection with Fig. 11 appears.

In panel d of Fig. 13 we show the velocity spectrum of O^+ scattered from helium. As expected, a sharp peak occurs at the velocity which corresponds to elastic scattering from mass 4. Notice that this peak is much narrower than the distribution of O^+ scattered from D_2, which clearly indicates that these latter collisions are not purely impulsive.

The angular distribution of the secondary inelastic feature which is evident in panels b and c of Fig. 13 appeared in Fig. 11. The fact that the ridge corresponding to this secondary feature is approximately concentric with the $O^+ - D_2$ center-of-mass suggests that it should be associated with an interaction of O^+ with the complete D_2 molecule, rather than with one atom. In Fig. 13d, a similar inelastic feature appears in the spectrum of O^+ scattered by He. This suggests that the feature in the $O^+ - D_2$ spectra should be associated with the excitation of O^+, at least in part.

We do not have sufficient information to make a definitive identification of these secondary inelastic features. However, the following observations may provide an indication of their nature. The secondary inelastic feature first appeared in an O^+ - H_2 experiment (not shown here) at 27.8 eV relative energy, and had a Q value of - 24 eV. The Q value of the inelastic peak in the O^+ - He experiment shown in Fig. 13d is - 23 eV. If these two features are of common origin, they must represent an excitation of O^+, and indeed the transition $O^+\ 2s^22p^3(^4S) \rightarrow O^+\ 2s^22p^23s(^4P)$ requires 22.96 eV. However, as the O^+ projectile energy is increased, the Q value of the secondary inelastic peak from O^+ - D_2 collisions decreases, reaching - 28 eV in Fig. 13b, and - 40 eV in Fig. 13c. This indicates that any excitation of O^+ is accompanied by an excitation to a continuum. The most likely possibility is the dissociation of D_2. It is also possible that at the highest relative energies, dissociation could be accompanied by ionization. For example, the process

$$O^+(^4S) + D_2 \rightarrow O^+(^4P) + D^+ + D + e$$

requires 41 eV, just the magnitude of the Q value of the two secondary features in Fig. 13c. We did observe a D^+ signal from O^+ - D_2 scattering at this energy in a region of velocity space which would not allow OD to be bound in its ground state. Thus dissociative charge transfer does

occur, and dissociative ionization accompanied by excitation of the projectile may occur, but the data we have are insufficient to permit more than a speculative description of the origin of the secondary inelastic feature.

Panels e - h of Fig. 13 show the velocity spectra of O^+ scattered from HD. At the lowest energy, only one peak is observed, but as the initial relative energy increases, the inelastic feature separates into two peaks. The maximum corresponding to scattering from the H atom falls exactly at the velocity predicted by the impulse model. In contrast, the scattering from the D atom maximizes at laboratory velocities slightly greater than predicted by the impulse model. This behavior is also evident in Fig. 12. Despite this deviation, the scattering of O^+ by HD provides a clear demonstration of the impulsive nature of the non-reactive collisions, somewhat modified by the effects of molecular binding.

Discussion

There are four major features of the behavior of this system with which a model for the reaction dynamics should be consistent:

1) There is a sudden disappearance of the product peak at 0° when the spectator stripping velocity passes into the region of velocity space where products are unstable. That is, there is no zero angle <u>recoil</u> of products in this system;

2) The product distributions from the homonuclear target molecules are very much alike, but differ greatly from the OH^+ and OD^+ distributions from HD. The latter are in turn markedly different from each other;

3) In the range of relative energies from 15 to 35 eV, the product velocity vector distributions change only slightly in form, but diminish greatly in intensity;

4) As the initial relative energy is increased above 10 eV, the large angle nonreactive intensity ridge becomes continuously narrower, and moves toward the locus of pure impulsive scattering.

The occurrence of spectator stripping at low relative energies, its loss at high energies, and the concomitant appearance of impulsive nonreactive scattering strongly suggest a potential energy surface which has certain regions where the motions of the three atoms are largely decoupled. On such a surface, the important changes in the velocities of pairs of atoms could come about through the impulsive interaction of their relatively hard spherical cores. In this picture, spectator stripping and impulsive inelastic scattering are seen as complementary two-body processes which involve little or no momentum transfer to the spectator atom. At low relative energies, it is possible to form stable product by a two-body interaction, but at

energies where Q_{ss} is more negative than the stability limit, these two-body interactions (and some others) lead to impulsive non-reactive scattering.

Pursuing this point of view, we are led to regard product formation (at least at high energies) as the result of two sequential two-body interactions: A hits B, B hits C, and A may combine with B or with C if the appropriate final relative translational energy is less than the corresponding bond energy of the product molecule. That is, in this model the attractive forces serve only to hold the reactant molecule together before reaction, and may do the same for the product molecule, but do not otherwise influence the trajectories. The second (B-C) impulse transfers some of the A - B relative energy to the freed atom, and may therefore lead to stable molecule formation at energies where spectator stripping can not. The interaction of B with C necessarily deflects the center-of-mass of the product molecule from the original direction of the projectile, and consequently reactive scattering at high energies appears only at nonzero angles. Since in an impulsive B-C interaction, the possible results depend only on the <u>ratio</u> of the masses and the initial relative velocity, it seems quite reasonable to expect that the final product angular distribution will depend sensitively on the B-C mass ratio, and less on their absolute values. Thus a sequential impulse model of the reaction is not only suggested by items 1 and 4 above, it also seems to have the features needed to explain items 2 and 3.

The sequential impulse model of Bates, Cook, and Smith[1] is an approximate treatment carried out under the assumption that the particles scatter in pairs according to the Rutherford differential cross section. The authors computed only the total cross section as a function of collision energy. George and Suplinskas[7,8] considerably refined and extended the model. They assumed that attractive ion-induced-dipole forces acted on both the incoming reactants and outgoing products, with hard sphere interactions connecting these asymptotic legs of the trajectory. Their computations of the energy and angular distribution of products of the $Ar^+(D_2,D)ArD^+$ are in good agreement with experiment at low relative energies, but are less successful at high (above 7 eV) relative energies.

To generate a sequential impulse model suitable for comparison to our data, it seems reasonable to ignore the ion-induced-dipole interactions. At internuclear separations where this potential is accurate, its magnitude is a minuscule fraction of the kinetic energy. At separations where it is of substantial size, the perturbation-point dipole assumptions inherent in its derivation are violated, and it can be accurate only by accident. The uninhibited use of this potential in ion-molecule problems should be avoided. It is also unlikely that, at the energies of our experiments, the Coulomb repulsion employed by Bates, Cook, and Smith[1] is an accurate representation of the forces between atomic cores.

A shielded Coulomb or simple exponential repulsion might be the most accurate approximation, but we choose the hard sphere potential instead. This potential has the virtues of enormously simplifying the problem both conceptually and computationally, and allowing us to explore the characteristics of the rigorous impulse limit. Finally, we shall ignore the 0.43 eV reaction exoergicity as being small compared to the kinetic energies employed. This choice also is consistent with the introduction of the hard sphere core potential.

Before exploring the product angular distributions predicted by the sequential impulse model, it is helpful to see how certain of its consequences can be deduced merely by using a compass and straightedge. Consider a stationary (in the LAB frame) molecule as the target of the projectile O^+, whose LAB velocity is $\underset{\sim}{V}_{O^+}$, the initial relative velocity of the collision. The projectile strikes the first deuterium atom (D1) impulsively and elastically. All the possible resulting velocities of O^+ and D1 lie on two concentric elastic spheres whose common origin is the velocity of the O^+-D1 center-of-mass, and whose radii are the initial speeds of O^+ and D1 relative to the O^+-D1 centroid. This construction is shown in Fig. 14a, where the intersections of the elastic spheres with the initial orbital plane of O^+ and D1 are shown as the circles labeled V'_{O^+}, V'_{D1}. (We adopt the convention of adding a prime to all velocities after each

impulsive interaction. Also, boldface symbols stand for particular values of the velocity vectors, and normal face is used to denote the locus of all possible such vectors.) After the initial O^+-D1 interaction is over, D1 moves toward the second deuterium atom (D2) with a relative velocity which is just $\underset{\sim}{V}'_{D1}$, the LAB velocity of D1 after the first impulse. The D1-D2 interaction merely rotates this velocity vector about the D1-D2 centroid velocity, which lies on $\underset{\sim}{V}'_{D1}$, a distance V'_{D1} (D1/(D1 + D2)) from the LAB origin. This produces another elastic sphere whose intersection with the orbital plane is shown in Fig. 14a as V''_D. If the target molecule had been HD, two concentric elastic spheres would have been generated, one for V''_H, the other for V''_D. It is important to realize that all velocities introduced so far can be expressed as multiples of V_{O^+}, and therefore, one diagram like Fig. 14a can describe all energies merely by a change of scale.

To decide whether a reaction has occurred, one can imagine that O^+ drags with it an imaginary capture sphere whose radius υ_c is the maximum velocity that D1 or D2 can have relative to O^+, and still be bound as OD^+. That is

$$\upsilon_c = \left(\frac{2\ D_o}{\mu}\right)^{1/2}$$

where D_o and μ are the appropriate dissociation energy and reduced mass respectively. It should be noted that this

capture velocity is a fixed number, and does not scale with V_{O^+}. Fig. 14b shows that for certain combinations of deflections, the velocity of either particle D1 or D2 may lie within the capture sphere. The specific case illustrated in Fig. 14b shows capture of what many might take to be the "wrong" particle, D2. The eventual velocity of the product molecule can be found by locating the velocity of its center-of-mass on the relative velocity vector of its constituent particles.

The procedure just outlined is the simplest way to decide whether a particular initial velocity and subsequent deflections will lead to reaction. However, to find the limits on the product angular distribution imposed by the kinematics, another closely related procedure is preferable. The construction, which applies to the $O^+(HD,D)OH^+$ reaction, is shown on Fig. 15. We begin by locating the O^+-D and O^+-H centroids (not shown) on the O^+ velocity vector, and then draw the elastic circles V'_{HKO} and V'_{DKO}. For clarity, only half of each circle is drawn, and thus the top half of the diagram represents events in which H is hit first, and the bottom those in which D is hit first. A full construction for both possibilities would, of course, be symmetric about $\underset{\sim}{V}_{O^+}$. At a convenient angular interval (15°) we draw from the origin to the appropriate elastic circle, two series of velocity vectors which represent specific values of $\underset{\sim}{V}'_{DKO}$ and $\underset{\sim}{V}'_{HKO}$. Each of these vectors

is divided at the appropriate centroid for the second (H-D) impulsive collision. With these centroids as origins, we draw a series of elastic circles which describe the possible results of the second impulsive collision. For clarity, only portions of these circles are shown in Fig. 15.

To find which of these second events produce reactive scattering, we overlay the diagram with a circular ring of velocities which has as its origin the center-of-mass of the complete target-projectile system. The outer and inner radii of this ring are defined for a particular isotopic freed atom by the maximum and minimum values of Q which permit stable product formation. That is, if the D atom is scattered into the stability ring of Fig. 15, energy and momentum conservation insure that the OH^+ product will be bound. Therefore, the segments of the arcs of the V''_D elastic circles which fall in the stability zone of Fig. 15 correspond to reactive events.

Figure 16 is a similar construction which applies to the $O^+(HD,H)OD^+$ reaction. The diagram is the same as that in Fig. 15, except that the stability zone for the free H atom lies at larger velocities than does the corresponding D atom stability zone. Because we have chosen to ignore the reaction exoergicity, the stability zones in Figs. 15 and 16 correspond to Q values of 0 eV (outer limit) and - 4.93 eV (inner limit), rather than the experimental limits of 0.43 and - 4.5 eV respectively. The full stability zones shown

are appropriate for collisions with an initial relative energy of 15.8 eV. However, the effect of changing the initial relative collision energy is easily represented. As the initial energy is increased, the velocity vectors can be regarded as being fixed in size, but changing in scale. The outer limit of the stability zone, or strictly the $Q = 0$ circle, also remains fixed in size, with the same change in scale. The inner limit of the stability zone increases in radius as the scale of the vectors changes with increasing energy, because the inner stability circle lies at a fixed relative energy from the $Q = 0$ circle. Thus as the initial energy increases, the stability zone is shaved away from the inside, and product formation becomes less probable.

Inspection of Figs. 15 and 16 shows that for certain results of the first impulse, there is no possible second impulse that can lead to a stable molecular product. Such collisions may be inelastic or dissociative, and contribute to the impulsive ridge of O^+ scattering. The events which do produce stable molecules put the freed atom into a well-defined range of angles. By inspection and testing, the first and last V'_D (or V'_H) vectors which permit scattering into the stability zone can be found. In the O^+-HD barycentric system, if the freed atom is found at $\pi-\theta$, the corresponding molecule will appear at θ. Thus from the angular range in which the free atom appears, the

corresponding range in which the molecule will be found can easily be inferred.

From Figs. 15 and 16, many of the major features of the experimental product distributions can be rationalized. Considering first the OH^+-D product pair (Fig. 15), we look for angular regions in which the D atom can be scattered into the stability zone. We see that some atoms can fall into angular interval 1, which lies in the large angle region of the O^+-HD barycentric system. This implies that OH^+ will appear with high intensity in the small angle region, but not right at zero degrees. We see that in this set of processes, H is the atom struck first by O^+. Only those O^+-H collisions in which the CM deflection angle ranges from small (but not zero) values to approximately 150° can lead to H-D collisions that produce stable product. These latter H-D interactions must produce deflections greater than zero, but the arcs in region 1 of Fig. 15 show that there is a considerable range of deflections which are acceptable. Thus, a rough description of this contribution to the reaction is that O^+ scatters off H, H hits D, undergoes a deflection and proceeds in the general direction of the O^+ to form OH^+ in the angular range from approximately 5 to 60°.

Reaction to form OH^+ can also occur if D is hit first and then scatters off H. Stable product is formed by this process in region 2 of Fig. 15, which covers a wide angular range. We see again that this process can not produce

OH^+ at 0°, but does lead to highly stabilized OH^+ which should appear in greatest intensity near 45°. However, product can also be formed at angles as large as 180° by scattering the D atom almost directly forward in the CM system and making only a grazing D-H collision. When the O^+-D scattering angle is 180°, and the subsequent D-H scattering angle is 0°, we have the ideal knockout process.[2] The low density of arcs in this region suggests that the backscattered OH product should be of low intensity, and this is observed experimentally. At 15.8 eV relative energy, the segments of the V''_D circles that correspond to the knockout process lie only slightly within the stability zone. As the initial collision energy is increased and the stability zone narrows, relatively less backscattered OH^+ will be formed, and this is also observed experimentally.

We turn now to Fig. 16, which is concerned with the formation of OD^+ and H. Considering collisions in which D is hit first and OD^+ is formed, we see that the H product must fall in region 3. The corresponding OD^+ product is therefore excluded from the small angle region, but appears at all larger angles, with greatest intensity near 90°. This is consistent with the experimental observations.

The velocity vectors $\underset{\sim}{V}'_D$ which can eventually lead to stable produce come from large (> 70°) deflections in the O^+-D CM system. The subsequent D-H collisions also must involve large deflections in order to place the final H velocity in the stability zone. Thus the reaction process

can be described as O^+ approaching DH with its velocity vector making a relatively small angle with respect to the D-H axis, and with a relatively small impact parameter. A large angle O^+-D deflection is followed by a large angle D-H deflection, and OD^+ is produced which appears over a wide range of angles, but most intensely at 90°.

When the H atom is hit first, reaction to form OD^+ must put the H atom velocity vector in region 4 of Fig. 16. This results in OD^+ appearing in the forward hemisphere of the CM system, with greatest intensity near 30°. Production of OD^+ at 0° is seen to be possible at 15.8 eV, but is not observed experimentally. For some of the scattering near 0°, the two-step sequential impulse picture is misleading, since a third impulse may occur. That is, for an exactly collinear O^+ - H-D collision, O^+ hits H head-on, H hits D and bounces back toward O^+, and a third (O^+-H) impulse occurs. The chance of these multiple collisions diminishes rapidly as the system departs from collinearity. In our investigations (see below) of the exact hard sphere trajectories in which the initial conditions were a properly weighted sample, we found that triple collisions occurred in only approximately 10% of the events.

The diagramatic method just described indicates the possible regions of product formation, but since it does not include weighting of collision parameters like

impact parameter and orientation angle, it can not provide detailed quantitative product distributions. Consequently, a computer program was written to sample a properly weighted set of 3-dimensional hard sphere collision events. The criteria for reaction were as described in connection with the velocity vector diagrams. The target atoms were taken to be motionless and separated by 0.75 Å. The hard sphere radii for the H and D atoms were chosen with the aid of the ground state potential energy curve[18] of H_2. Values of the average energy with which two H (or D) atoms collide in our experiments were found, and a range of corresponding internuclear separations was read off the H_2 potential energy curve. This led to 0.12 to 0.25 Å as the range of H atom radii. Corresponding O^+ radii were then found in a similar manner by using an extrapolation of the $OH^+(^3\Sigma^-)$ curve computed by Stevens and Wahl.[19] This led to O^+ hard sphere radii in the range 0.32 - 0.42 Å. The shape of the angular distribution was not particularly sensitive to the values chosen for the radii, but was more affected by r_H than by r_{O^+}. The results presented here were obtained with r_H = 0.25 Å, and r_{O^+} = 0.40 Å, which produced the best agreement with experimental angular distributions.

For the system O^+-D_2 at 20 eV relative energy, Fig. 17 shows a comparison of the experimental and calculated angular distributions, which are defined by

$$I(\theta) = \int_0^\infty \bar{I}(u,\theta)u^2du$$

The intensity is given in arbitrary units, and the height of the experimental distribution has been adjusted by multiplying by the ratio of the calculated to experimental relative total cross sections. The calculated differential cross section is somewhat shifted to smaller angles than the experiment, but the agreement between the shapes is quite good. The partial cross sections for reaction with the atom hit first (shaded bars) and hit second (open bars) are nearly the same at all angles. This is perhaps not too surprising, considering the symmetry of the D-D scattering process.

The product distributions from O^+-HD collisions provide a particularly demanding test of the model. In Fig. 18 we compare the experimental and calculated differential cross sections for forming OH^+ from O^+-HD collisions at 15.8 eV initial relative energy. The agreement is very good, except at small angles, where the calculated values are too large. It is of interest that the reaction processes which contribute at small and large scattering angles are quite different, as Fig. 15 suggested. At small angles, reaction is principally with the atom which is struck first (zone 1 of Fig. 15). For product at large angles, the D atom is hit first, and it grazes the H atom, which is then picked up by the O^+ (zone 2). In essence, knockout processes are responsible for the large angle reactive scattering at this energy.

Figure 19 shows a comparison between the experimental and calculated OD^+ distributions for 15.8 eV collisions. At large angles, where the principal contribution to the differential cross section is reaction with the first atom struck, the agreement between the experiment and the calculation is quite good. At small angles, however, the calculated values considerably exceed the experiment. The excess comes almost exclusively from the contribution of the process in which O^+ hits H, H makes nearly a head-on collision with D, and is then scattered back to large angles, while O^+ and D proceed together to small angles.

It is curious that a model composed of hard spheres should err by placing too much product intensity in the small angle region. Some illumination of this point comes from an examination of the calculated product intensity contour map in Fig. 20. Both the OH^+ and OD^+ distributions are shown, and these correspond to the experiments of Fig. 5 and 6 respectively. It is clear that both the OH^+ and OD^+ products formed at very small angles are highly excited internally. The OD^+ in particular has its maximum intensity right at the stability limit. Rather slight perturbations due to the neglected attractive walls of the potential could move much of this zero-angle intensity into the unstable region, or out to larger angles.

The possibility of such an effect in the $O^+(HD,H)OD^+$ reaction becomes evident upon examination of the atom

trajectories. As stated above, the major contributor to OD^+ product at small angles is a process in which O^+ hits H and scatters it forward; H hits D and is scattered backward while O^+ and D proceed forward. As H moves backwards on the final leg of the trajectory, it passes rather close to the forward moving O^+, while the D atom is still at a substantial distance from both O^+ and H. In this interval, there is very probably a strong attractive bonding force between O^+ and H. Any such attractive O^+-H force would act to decrease the laboratory velocity of O^+, and would scatter the H-product out of the backward region. A strong attractive interaction would either increase the O^+-D relative velocity to the point of the product instability, or would surely rotate the OD^+ trajectory away from the very small angle region.

In a somewhat similar way, attractive forces can remove some of the OH^+ from the small angle region. In the principal reactive process in this case, O^+ hits H in a glancing collision, giving it a rather small velocity in a direction nearly perpendicular to the original projectile velocity. This H atom then moves slowly toward D, makes a large deflection in the forward direction, and tries to follow the O^+. Any residual bonding attraction between the H and D will decrease the laboratory velocity of H, and thereby increase the O^+-H relative velocity. The result may be dissociation of an ion which otherwise would

have appeared (highly excited) in the very small angle region.

It seems possible to account for the major errors in the product angular distributions predicted by the sequential impulse model in the relative energy range from 15 to 32 eV by introducing the most basic consequences of attractive forces. In a like manner, the deviations of the inelastic scattering from the exact impulse model can be rationalized, and the details of the arguments need not be presented here.

A comment is in order concerning the consequences of neglecting the 0.43 eV exoergicity of the reaction. To see how inclusion of this factor might affect the angular distributions, we can use the construction of Fig. 15. Taking account of the exoergicity would cause the outer and inner limits of the stability zone to expand to velocities which correspond to Q values of 0.43 and - 4.5 eV respectively, which is a very slight change. Some decision about how the exoergicity is to be divided between the two impulsive interactions must be made. If it is released entirely as O^+ interacts with the atom (let us say H) it strikes first, the "elastic" circle which described V'_H is correspondingly expanded. The magnitude of this change is small compared to the already large V'_H, and tends to offset the effect produced by the outward expansion of the stability zone. Thus inclusion of the reaction exoergicity in this manner has virtually no effect on the product angular distribution.

If the exoergicity is released entirely on the outgoing leg of the trajectory, that is, as H-D repulsion, the situation is a bit more complicated. If, as a result of the O^+-H collision, $\underset{\sim}{V}'_H$ is large the fractional increase in its magnitude which occurs when it is expanded by the contribution from the reaction exoergicity is relatively small, and has little effect on the product angular distribution. The situation is quite different when $\underset{\sim}{V}'_H$ is small, however. Then, the reaction exoergicity can expand the D-H relative velocity vector by a large factor, and recoil of the D atom into the stability zone becomes possible. That is, this type of energy release makes possible backward recoil of the D atom and forward (small angle) recoil of stable OH^+. If this were to occur, a product peak could be found at zero degrees even when the <u>spectator</u> stripping velocity lay in the unstable region of velocity space. The fact that this is not observed experimentally in the O^+-H_2 system suggests that the exoergicity is released principally during the incoming, rather than the outgoing, leg of the trajectory. Since, as we have argued, this early energy release has little effect on the product angular distribution at high energies, ignoring the energy release in our model calculations seems justified.[20]

There is a serious discrepancy between the predictions of the impulse model and the behavior observed in the product distributions at 38.1 and 50 eV, Figs. 3

and 4. From a velocity vector construction for the O^+-D_2 case, one finds that as the limit of very high initial relative energy is approached, the OD^+ product distribution should contract to a peak at a barycentric angle of 56°. (This high energy limiting angle may be found most readily as the point of intersection of the Q = 0 circle for OD^+ and the elastic circle for O^+ recoiling from D.) In contrast, the experiments at 38.1 and 50.0 eV showed product only at angles greater than 90°. It is likely that the failure of the impulse model is caused by the assumption of the hard sphere potential, which becomes unrealistic at these highest energies. Calculations with a Born (shielded Coulomb) potential indicate that in the 38 and 50 eV experiments, a head-on O^+-D collision has a turning point at a 0.56 to 0.53 Å internuclear separation. Since this is less than the equilibrium D-D internuclear separation, it is hard to maintain that in all collisions in this energy range, the O^+ interacts with only one deuterium atom at a time. Moreover, the picture is further complicated by the likely intervention of excited electronic states, since it is in this energy range that electronic inelasticity is observed in the non-reactive scattering. In the light of these considerations, the failure of the model at very high energies is not particularly surprising.

There are two other instances in which the sequential impulse model fails. The experimental total reaction cross section decreases by a factor of 250 as the

relative energy is increased from 10 to 50 eV. In contrast, the calculated reaction cross section decreases by only a factor of 10 over the same range. This discrepancy can be diminished by allowing the hard sphere radii to decrease as the total collision energy increases. Indeed, the total cross section calculated by Bates et al[1] with Rutherford differential cross sections proportional to E^{-2} produced total cross sections which varied as $E^{-11/2}$. Our experimental total cross sections vary as $E^{-7/2}$, which probably could be reproduced with a potential somewhat stiffer than the Coulomb potential. However, it seems rather pointless to make this modification while still ignoring attractive forces.

The other major failing of the impulse model is its inability to reproduce the intramolecular isotope effect in the total cross section of the O^+-HD reaction. The experimental results are given in Table 1. The calculation yields $\sigma_{OH^+}/\sigma_{OD^+} = 1.0 \pm 0.1$ over the energy range from 15.8 to 40 eV. If one neglects the small angle OD^+ which comes from the O^+ hits H, H hits D process discussed above, the calculated isotope ratios are 2.1 ± 0.1 over the same range. If the radii of the hard spheres are allowed to diminish with energy, the calculated isotope effect shows a slight energy dependence, but in the sense opposite to the experimental trend. The correct isotope effect evidently can not be obtained without introducing attractive forces.

The successes and the failures of the sequential impulse model in its application to high energy collisions of O^+ with H_2, D_2, and HD have been very edifying. The manner in which the mass ratio of the target atoms determines the gross features of the angular distribution has been made particularly clear. The necessity for some feature which permits forward recoil of the product if zero angle scattering is to be maintained above the spectator stripping stability limit has become clearer. The velocity vector diagrams also clarify the nature of the spectator stripping process at intermediate (3-8 eV) energies. In order for product to be found at the spectator stripping velocity, it is the second or final state interaction which must vanish, while the first collision of the projectile with the atom it abstracts must involve an impact parameter small enough so that an acceleration of the abstracted atom away from the spectator atom occurs. Thus the assertion that stripping processes in this energy range involve grazing collisions is to be understood in the sense that it is the final, not necessarily the initial impact parameter, which must be large. The reason for the relative unimportance and the eventual high energy failure of the ideal knockout model or any close approximation to it has also been made apparent. Even in the most favorable case, where O^+ knocks out D and attempts to pick up H, the knockout process gives only a small amount of very highly excited product spread thinly over the large angle region. Highly stabilized OH^+

product is only possible through a collision sequence involving 60° - 120° scattering of O^+ off D followed by 60° - 90° scattering of D off H, and this sequence puts the OH^+ at angles of 90° or smaller in the center-of-mass system.

The sequential impulse model and the velocity vector technique of Fig. 15 and 16 are not limited to high energy applications. Used with increasing caution at decreasing energies, they can provide the basis for a more rational simple analysis of reactive scattering than has been available in the past. The points of caution are clear, and include the increasing importance of reaction thermochemistry at decreased energies as well as consideration of attractive forces and related features in the potential energy surface.

Acknowledgements: This work was supported by the U. S. Atomic Energy Commission. K. T. G. acknowledges financial support from the Miller Institute for Basic Research and the IBM Corporation and J. S. W. acknowledges predoctoral fellowship support from the National Science Foundation and the Proctor and Gamble Company.

References

1. D. R. Bates, C. J. Cook, and F. J. Smith, Proc. Phys. Soc. (London) 83, 49 (1964).
2. J. C. Light and J. Horrocks, Proc. Phys. Soc. (London) 84, 527 (1964).
3. R. J. Suplinskas, J. Chem. Phys. 49, 5046 (1968).
4. P. J. Kuntz, Trans. Faraday Soc. 66, 2980 (1970).
5. D. T. Chang and J. C. Light, J. Chem. Phys. 52, 5687 (1970).
6. R. Grice and D. R. Hardin, Mol. Phys. 21, 805 (1971).
7. T. F. George and R. J. Suplinskas, J. Chem. Phys. 54, 1037 (1971).
8. T. F. George and R. J. Suplinskas, J. Chem. Phys. 54, 1046 (1971).
9. M. T. Marron, J. Chem. Phys. 58, 153 (1973).
10. D. J. Malcolme-Lawes, J. Chem. Phys. 57, 5522 (1972).
11. K. T. Gillen, B. H. Mahan, and J. S. Winn, J. Chem. Phys. 58, 5373 (1973).
12. K. T. Gillen, B. H. Mahan, and J. S. Winn, Chem. Phys. Letters (1973).
13. H. H. Harris and J. J. Leventhal, J. Chem. Phys. 58, 2333 (1973).
14. F. C. Fehsenfeld, A. L. Schmeltekopf, and E. E. Feguson, J. Chem. Phys. 46, 2802 (1967).
15. M. H. Chiang, B. H. Mahan, C. W. Tsao, and A. S. Werner, J. Chem. Phys. 53, 3752 (1970).
16. M. Chiang, E. A. Gislason, B. H. Mahan, C. W. Tsao, and A. S. Werner, J. Chem. Phys. 52, 2698 (1970).

17. M. H. Chiang, E. A. Gislason, B. H. Mahan, C. W. Tsao, and A. S. Werner, J. Phys. Chem. 75, 1426 (1971).

18. T. E. Sharp, "Potential Energy Diagram for Molecular Hydrogen and its Ions", Lockheed Missiles and Space Co. Report 5-10-69-9, Palo Alto, Calif. 1969 (unpublished).

19. W. Stevens and A. C. Wahl, (private communciation).

20. It is of interest to note that at energies higher than the critical value at which spectator stripping must cease, the reactions $Ar^+(D_2,D)ArD^+$, $N_2^+(D_2,D)N_2D^+$, and $CO^+(D_2,D)DCO^+$ do show stabilization[16,21,22] of product at zero degrees by forward recoil of the molecular ion. These reactions are all significantly more exoergic (~ 1.4 eV) than the $O^+(H_2,H)OH^+$ reaction, and in high energy collisions can evidently release much of this energy on the outgoing leg of the trajectory.

21. W. R. Gentry, E. A. Gislason, B. H. Mahan, and C. W. Tsao, J. Chem. Phys. 49, 3058 (1968).

22. K. Lacmann and A. Henglein, Ber. Bunsenges. Phys. Chem. 69, 292 (1965).

Table I

Experimental Intramolecular Isotope Effects

E_{rel} (eV)	6.3	11.9	15.8	19.7
$\sigma_{OH^+}/\sigma_{OD^+}$ [a]	0.37	0.98	1.4	2.5

(a) Ratio of the total cross sections for isotopic product formation from O^+-HD collisions obtained by integration of the experimental velocity vector distributions.

Figure Captions

Fig. 1. A contour map of the specific intensity of OD^+ from O^+-D_2 collisions at 20.0 eV initial relative energy. The large circles labeled $Q = 0.43$ and $Q = -4.5$ eV give respectively the greatest and least speeds at which OD^+ is stable in its ground electronic state. The small cross locates the velocity which OD^+ would have if it could be formed by the spectator stripping process.

Fig. 2. A contour map of the specific intensity of OD^+ from O^+-D_2 collisions at 32.0 eV initial relative energy. Note the overall resemblance to Fig. 1, but also the increased prominence of scattering near 180°.

Fig. 3. The specific intensity of OD^+ from O^+-D_2 collisions at 38.1 eV initial relative energy. Note the absence of the intensity maxima in the small angle region which were evident at lower energies.

Fig. 4. The specific intensity of OD^+ from O^+-D_2 collisions at 50.0 eV initial relative energy. Note the very small overall intensity, the broad (in angle) intensity maxima near ± 150°, and the apparent tendency of the product near 180° to lie in regions of velocity space where only electronically excited products could be stable.

Fig. 5. A contour map of the specific intensity of OH^+ from O^+-HD collisions at 15.8 eV initial relative energy. Note the intensity maxima at $\pm$ 35°, and the very low intensity of product at angles greater than 90°. At small angles, there is noticeable intensity at speeds where $Q < -4.5$ eV; that is, where $OH^+(^1\Delta)$ may be stable, but $OH^+(^3\Sigma)$ is not.

Fig. 6. A contour map of the specific intensity of OD^+ from O^+-HD collisions at 15.8 eV initial relative energy. Note the complete absence of product from the very small angle region, and the rather slight variation in intensity at angles between 90° and 180° degrees.

Fig. 7. The specific intensity of OH^+ from O^+-HD collisions at 19.7 eV initial relative energy. Note the very close similarity to Fig. 5.

Fig. 8. The specific intensity of OD^+ from O^+-HD collisions at 19.7 eV initial relative energy. Note the close similarity to Fig. 6, and the contrast with Fig. 7.

Fig. 9. A contour map of the specific intensity of O^+ scattered from D_2 at 20.1 eV initial relative energy. Note that the small angle (< 45°) scattering follows the circle for elastic scattering from D_2 fairly closely. The scattering at larger angles is very inelastic, and tends to follow the "knockout circle"; that is, the locus of elastic scattering of O^+ from a free D atom.

Fig. 10. A contour map of the specific intensity of O^+ scattered from D_2 at 35.0 eV initial relative energy. Note that at this higher energy the large angle scattering follows the knockout circle (V_{KO}) more closely than was the case in Fig. 9. Note also that at 180°, a secondary inelastic feature is just starting to appear. This feature is more evident at higher energies (see Figs. 11 and 13).

Fig. 11. A contour map of the specific intensity of O^+ scattered from D_2 at 50.0 eV initial relative energy. Much of the inelastic scattering follows the knockout circle (V_{KO}) quite closely. The secondary inelastic feature which appeared in Fig. 10 is now clearly evident as a small ridge near 180°. The small crosses give the location of the intensity maximum of this ridge.

Fig. 12. A contour map of the specific intensity of O^+ scattered from HD at 27.6 eV initial relative energy. The inelastically scattered O^+ has a particularly broad speed distribution, and along the 0° - 180° axis, separates into two ridges. One of these ridges falls quite near to the knockout circle for scattering from a free H atom, and the other intensity ridge lies in the vicinity of, but at somewhat smaller speeds (in the barycentric system) than the knockout circle for scattering from a free D atom.

Fig. 13. Profiles of the intensity of O^+ scattered along the 0° - 180° axis in the atom-molecule center-of-mass system. In each panel the abscissa is the laboratory velocity of the ion, increasing from left to right. The label B locates the beam velocity; CM, the center-of-mass velocity; V_{D_2}, the velocity of O^+ scattered elastically from a particle of mass 4; V_{HD}, the velocity of O^+ scattered elastically from a particle of mass 3; V_D, the velocity of O^+ scattered elastically from a free D atom, and similarly for V_H. The initial relative energy and the collision system are given in each panel. All curves are normalized to the highest point measured in each run.

Fig. 14. Velocity vector constructions for the sequential impulse model of the $O^+(D_2,D)OD^+$ reaction at 20 eV initial relative energy. In (a), the elastic circles for the projectile (V'_{O^+}) and struck atom (V'_{D1}) are shown, along with a set of particular values $\underset{\sim}{V}'_{O^+}$, $\underset{\sim}{V}'_{D1}$ for these velocities. Also, the locus of final velocities (in the orbital plane) for D1 and D2 after their collision is shown as V''_D. In (b), a particular set of final velocities $\underset{\sim}{V}''_{D2}$ and $\underset{\sim}{V}''_{D1}$ is chosen, and it is seen that $\underset{\sim}{V}''_{D2}$ falls within the capture circle V_C centered on $\underset{\sim}{V}'_{O^+}$. Thus stable OD^+ is formed in this particular collision sequence.

Fig. 15. A velocity vector construction for the sequential impulse model of the $O^+(HD,D)OH^+$ reaction. In the upper half of the drawing, one half of the elastic circle for an H atom struck by $O^+(V'_{HKO})$ is shown, and in the lower half, the elastic circle for a D atom struck by $O^+(V'_{DKO})$ appears. The outermost heavy circle labeled $Q = 0$ represents the greatest speed at which D can be formed. The inner heavy circle represents speeds corresponding to $Q = -4.93$ eV for a collision in which the initial relative energy is 15.8 eV. Other short arcs in the upper right region give the location of this inner limit ($Q = -4.93$ eV) for the other initial relative energies indicated. In region 1, D appears (and OH^+ is therefore stable) after O^+ hits H first, then H hits D. In region 2, D again appears (and OH^+ is again stable) after O^+ hits D first, then D hits H. Note the considerable stability achieved by scattering D backwards and hence OH^+ forward in the barycentric system.

Fig. 16. A velocity vector construction for the sequential impulse model of the $O^+(HD,D)OD^+$ reaction. As in Fig. 15, only one half of the O^+-H and O^+-D elastic knockout circles are shown (V'_{HKO} and V'_{DKO} respectively). The outermost full circles locate the stability zone for H atoms from a 15.8 eV O^+-HD collision. In the upper right, the short arcs give the location of the inner limit of the stability zone for other initial relative energies. In region 3, H atoms appear (and OD^+ is therefore stable) when O^+ first hits

D, and then D hits H. In region 4, H atoms appear (and OD^+ is therefore stable) when O^+ first hits H, and then H hits D.

Fig. 17. Experimental and calculated product angular distributions for the reaction $O^+(D_2,D)OD^+$ at 20 eV initial relative energy. The smooth curve is obtained by integration of the data in Fig. 1. The histogram gives the results of a complete 3-dimensional sequential impulse model calculation. The shaded bars represent reaction with the atom first struck by the projectile, and the open bars represent the contribution from reaction with the second or trailing atom. The ordinate is in arbitrary units.

Fig. 18. Experimental and calculated product angular distributions for the $O^+(HD,D)OH^+$ reaction at 15.8 eV initial relative energy. The experimental results were obtained by integration of the data in Fig. 5. The notation and labeling are as in Fig. 17. Note that the calculations indicate that the large angle scattering comes exclusively from reaction with the second or trailing atom.

Fig. 19. Experimental and calculated product angular distributions for the $O^+(HD,H)OD^+$ reaction at 15.8 eV initial relative energy. The experimental results were obtained by integration of the data in Fig. 6. The notation and labeling are as in Fig. 17. Note that the discrepancy between the

calculation and experiment at small angles comes almost exclusively from contribution of the process in which O^+ first hits H, H hits D, and O^+ and D combine.

Fig. 20. Calculated contour maps of the product specific intensity for the $O^+(HD,D)OH^+$ and $O^+(HD,H)OD^+$ reactions at 15.8 eV initial relative energy. Note the very high product internal excitation in the very small angle region. Intensity contours have been extrapolated from 170° to 180°.

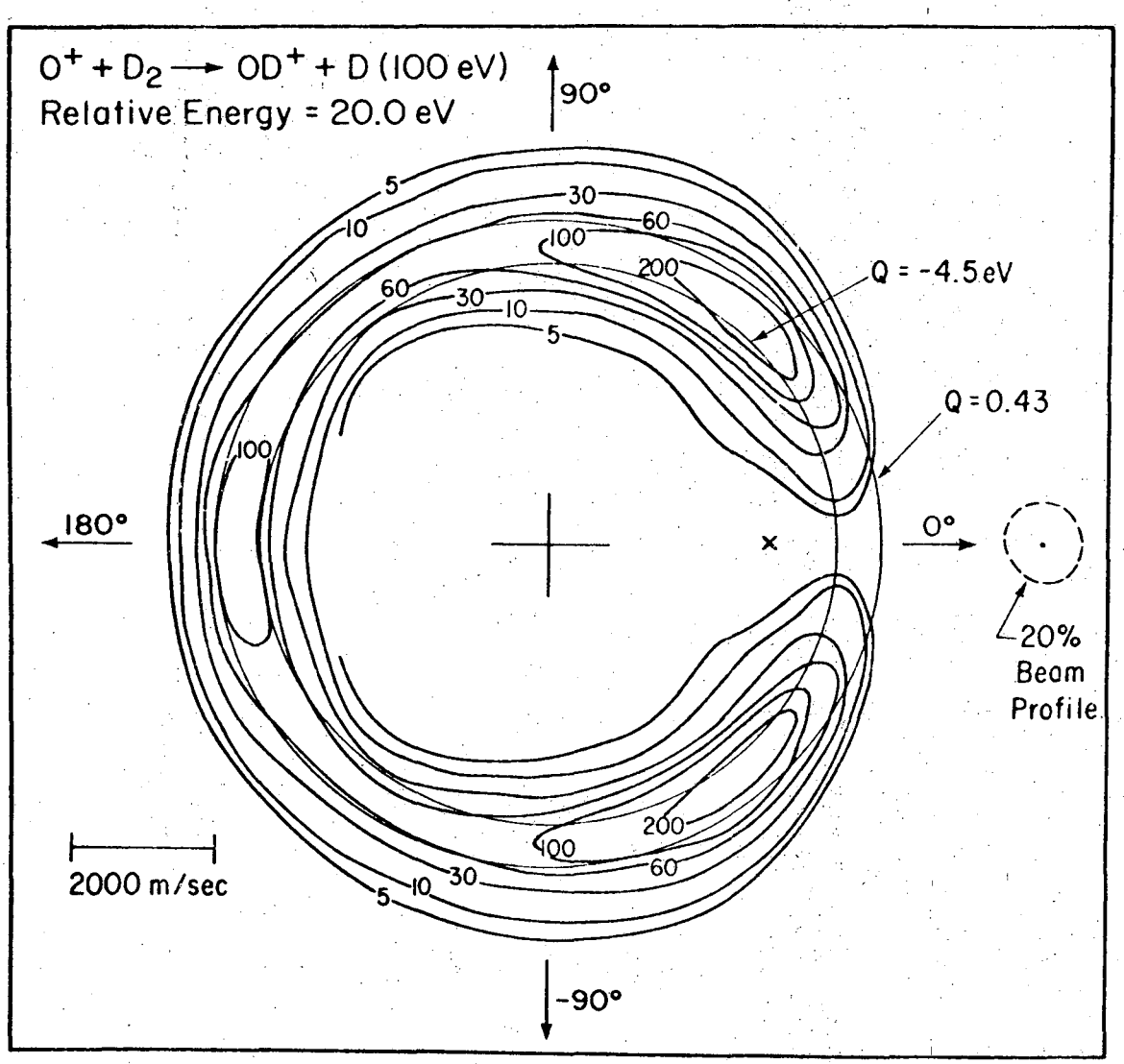

XBL727-6592

Fig. 1

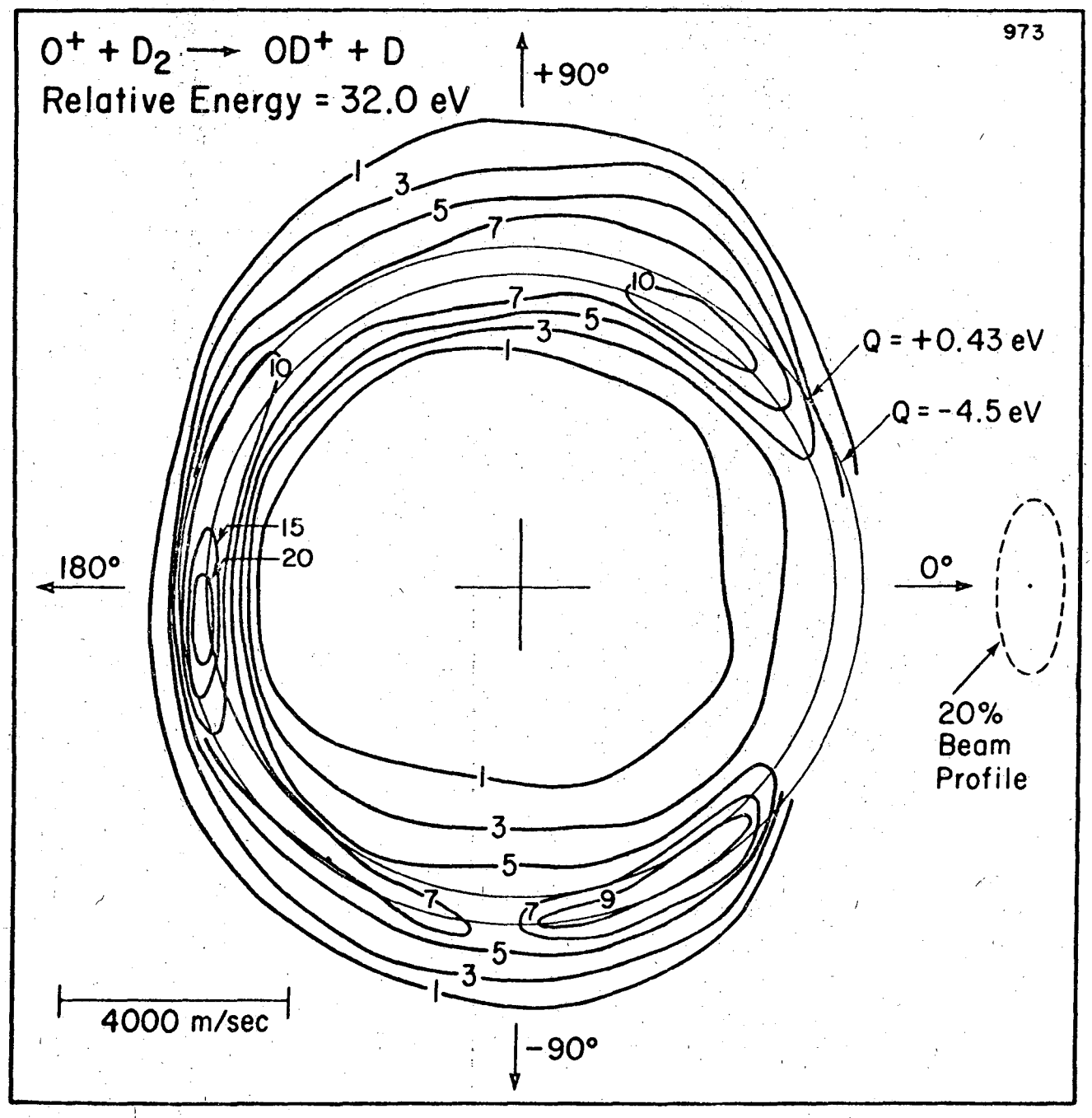

XBL 739-1908

Fig. 2

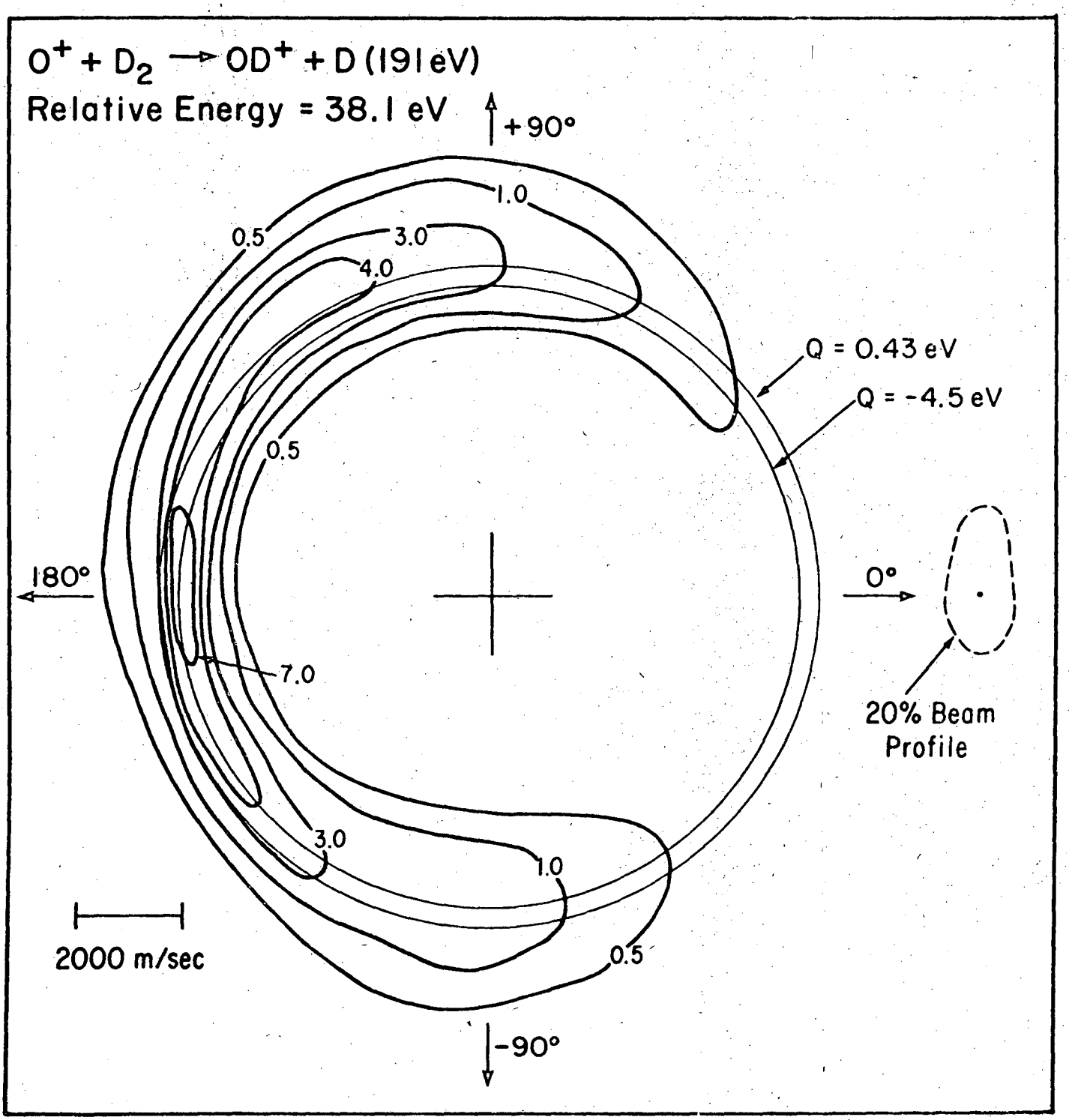

XBL 735-6134

Fig. 3

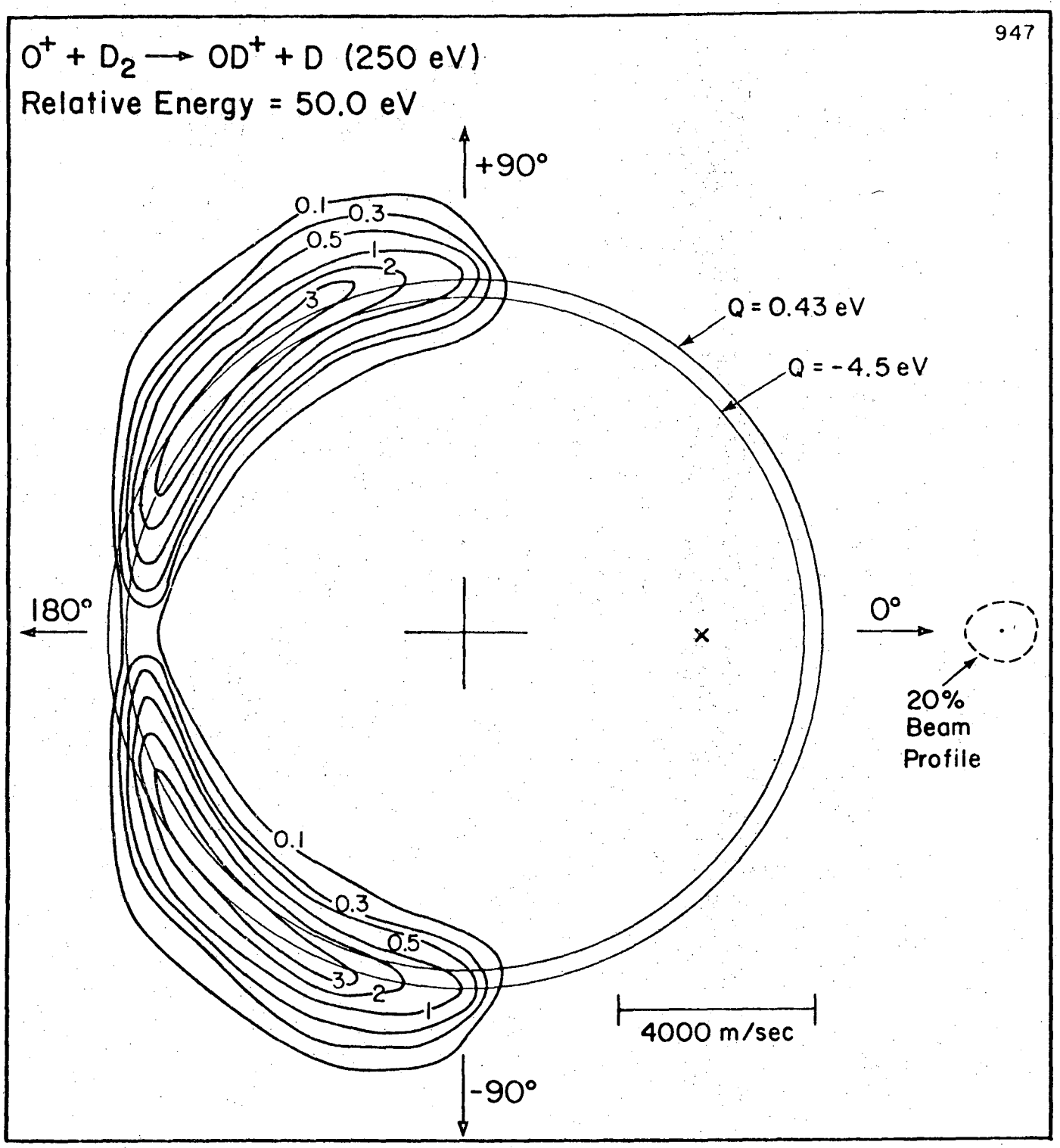

XBL 729-6914

Fig. 4

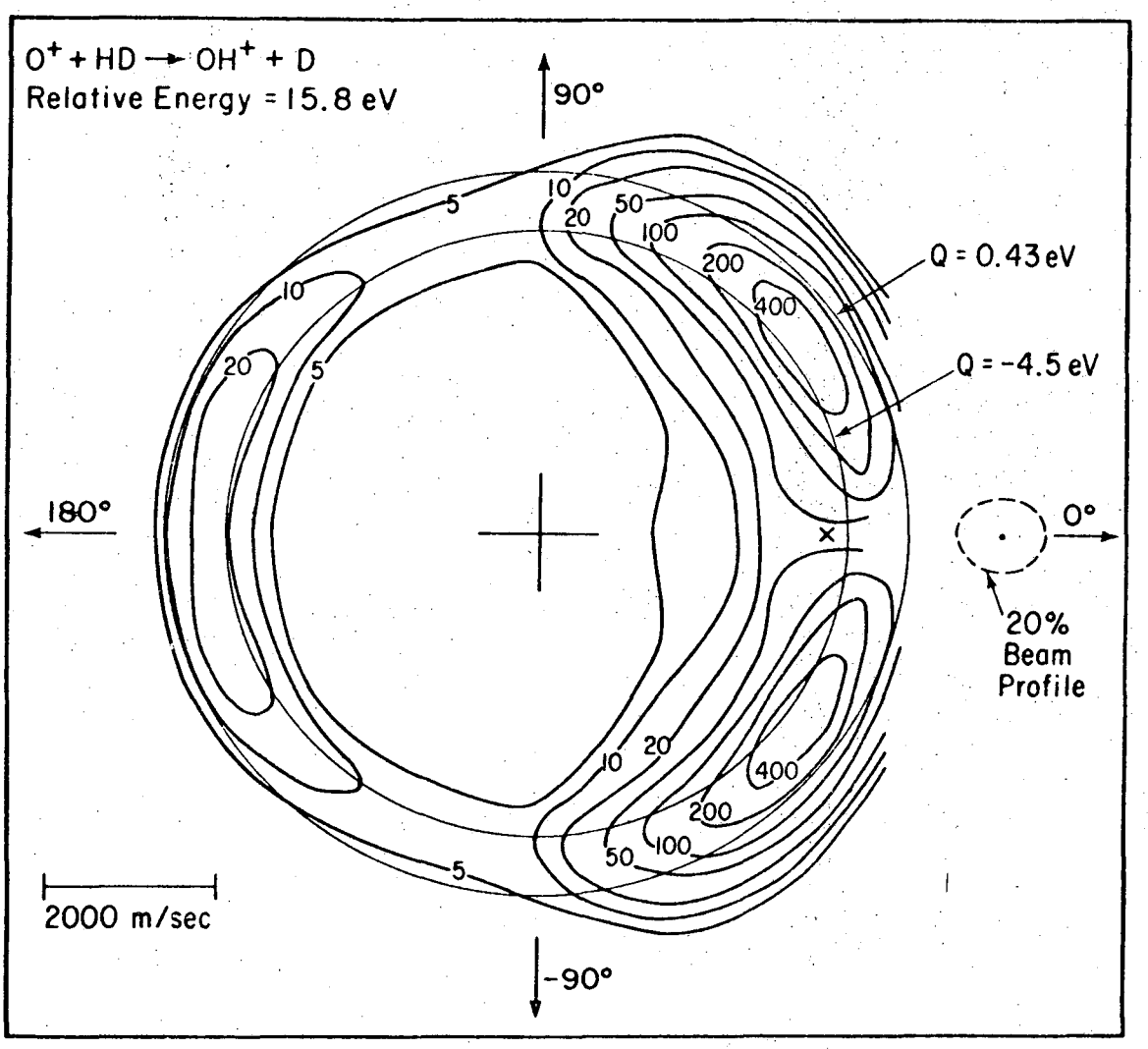

XBL727-6590

Fig. 5

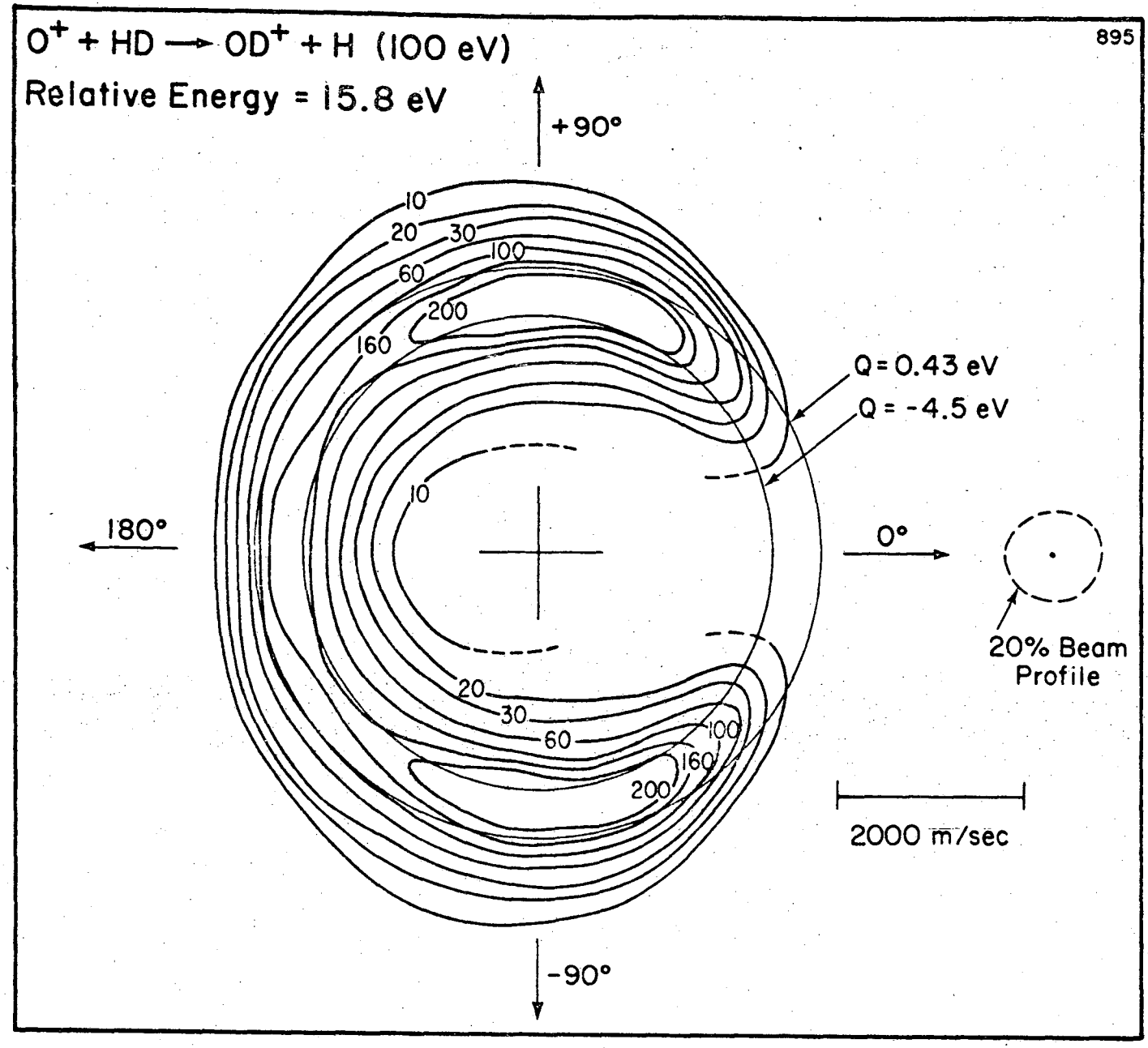

Fig. 6

XBL 728-6816

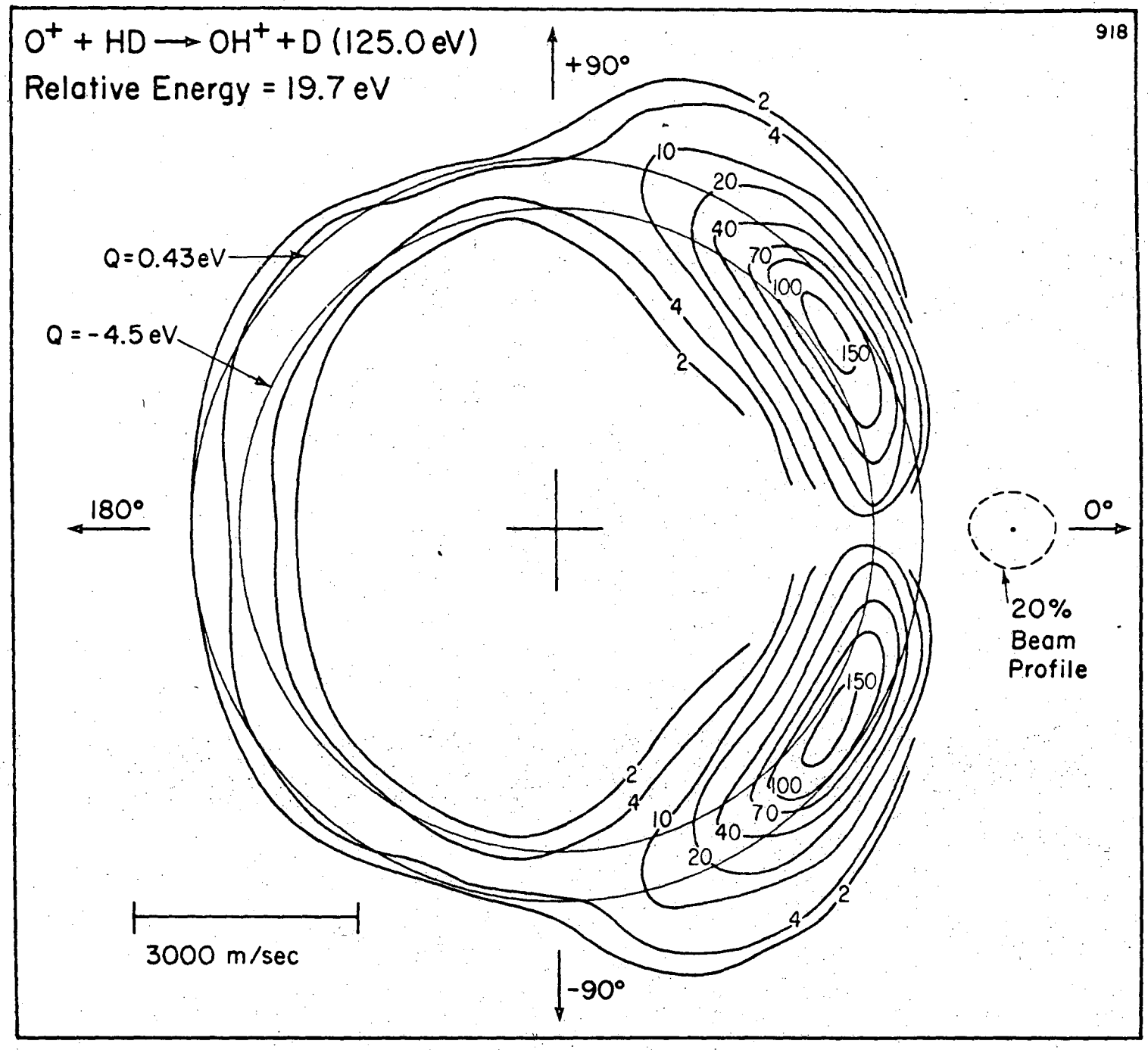

Fig. 7

XBL 728-6809

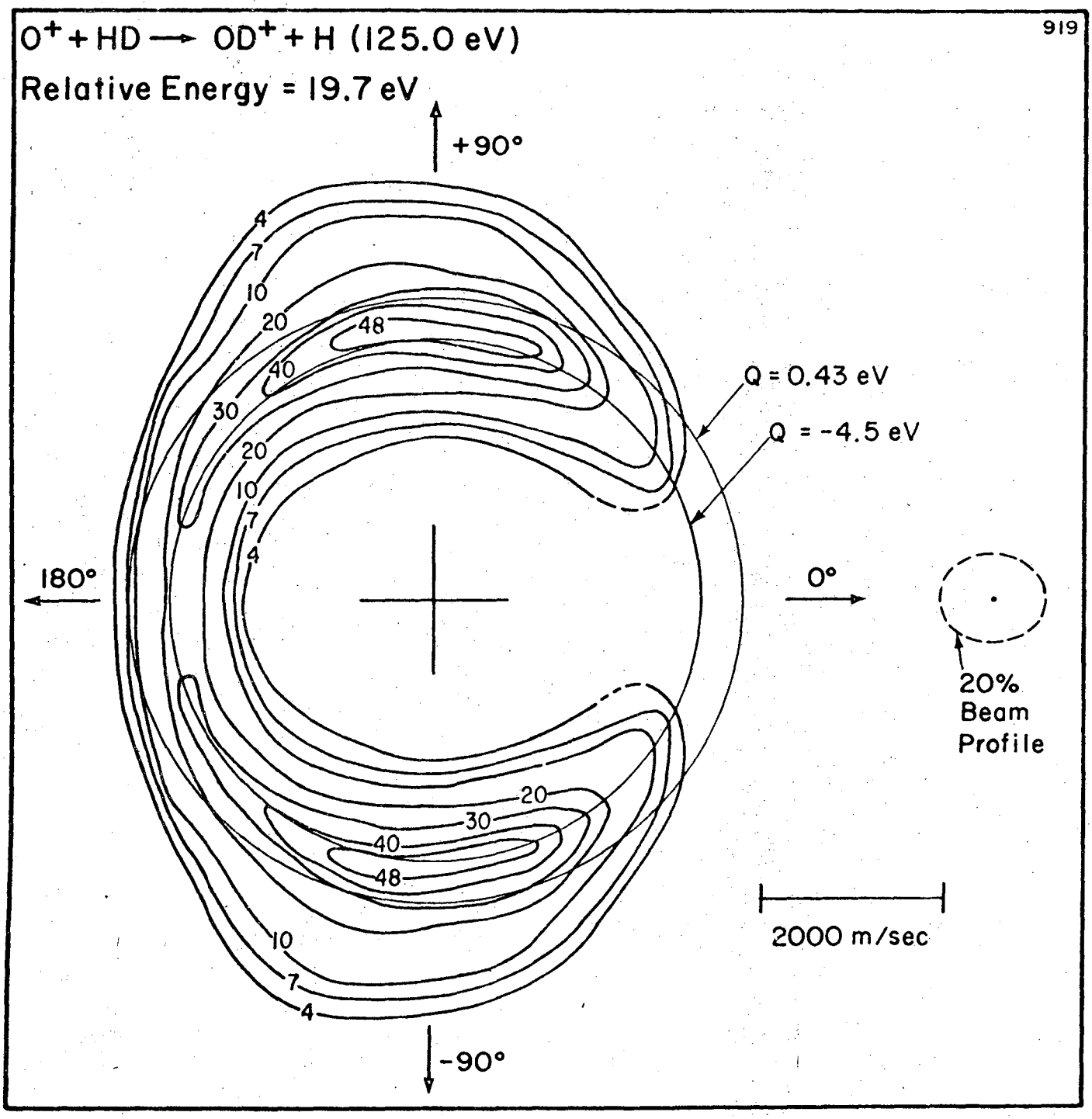

XBL 728-6811

Fig. 8

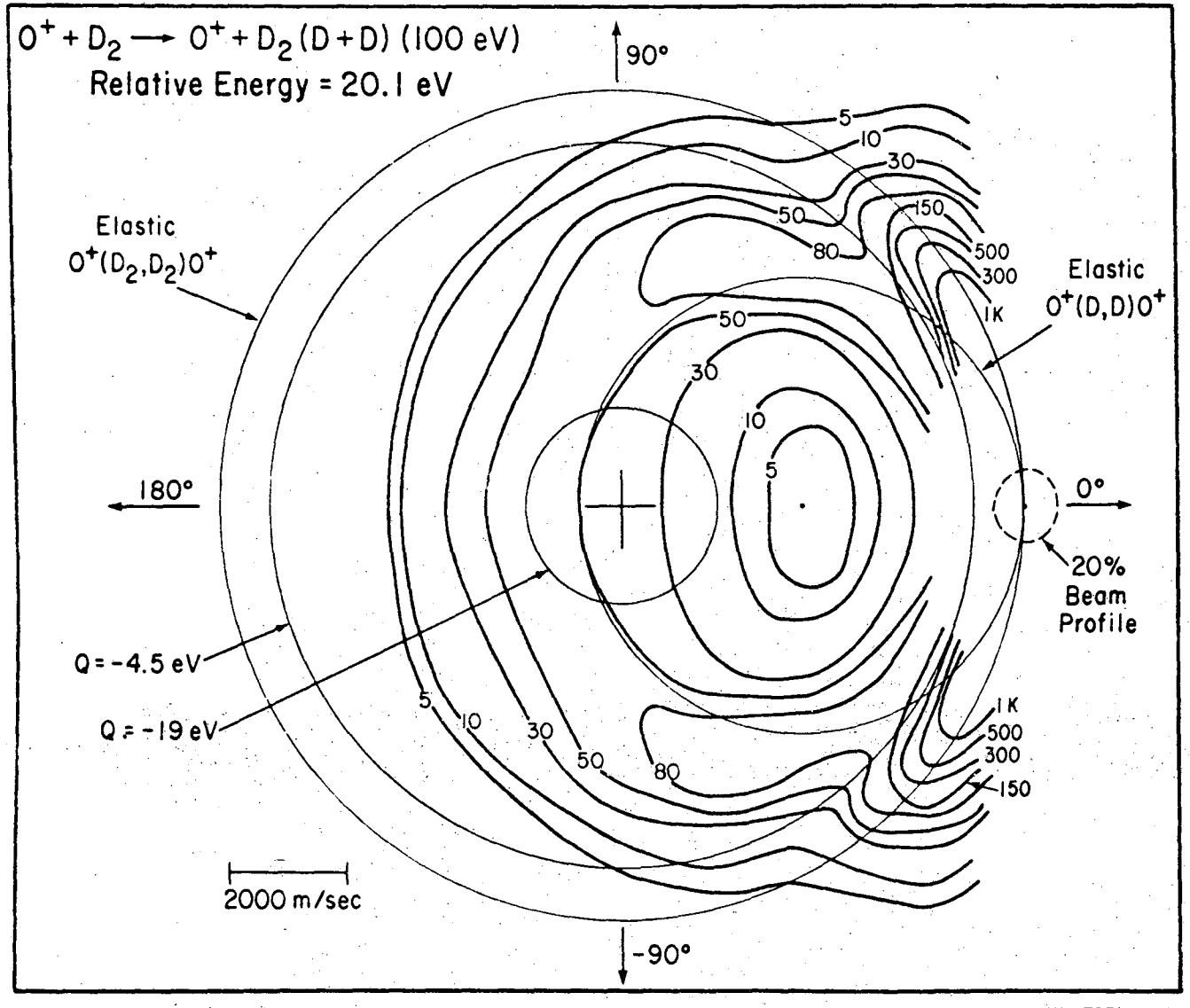

XBL727-6587

Fig. 9

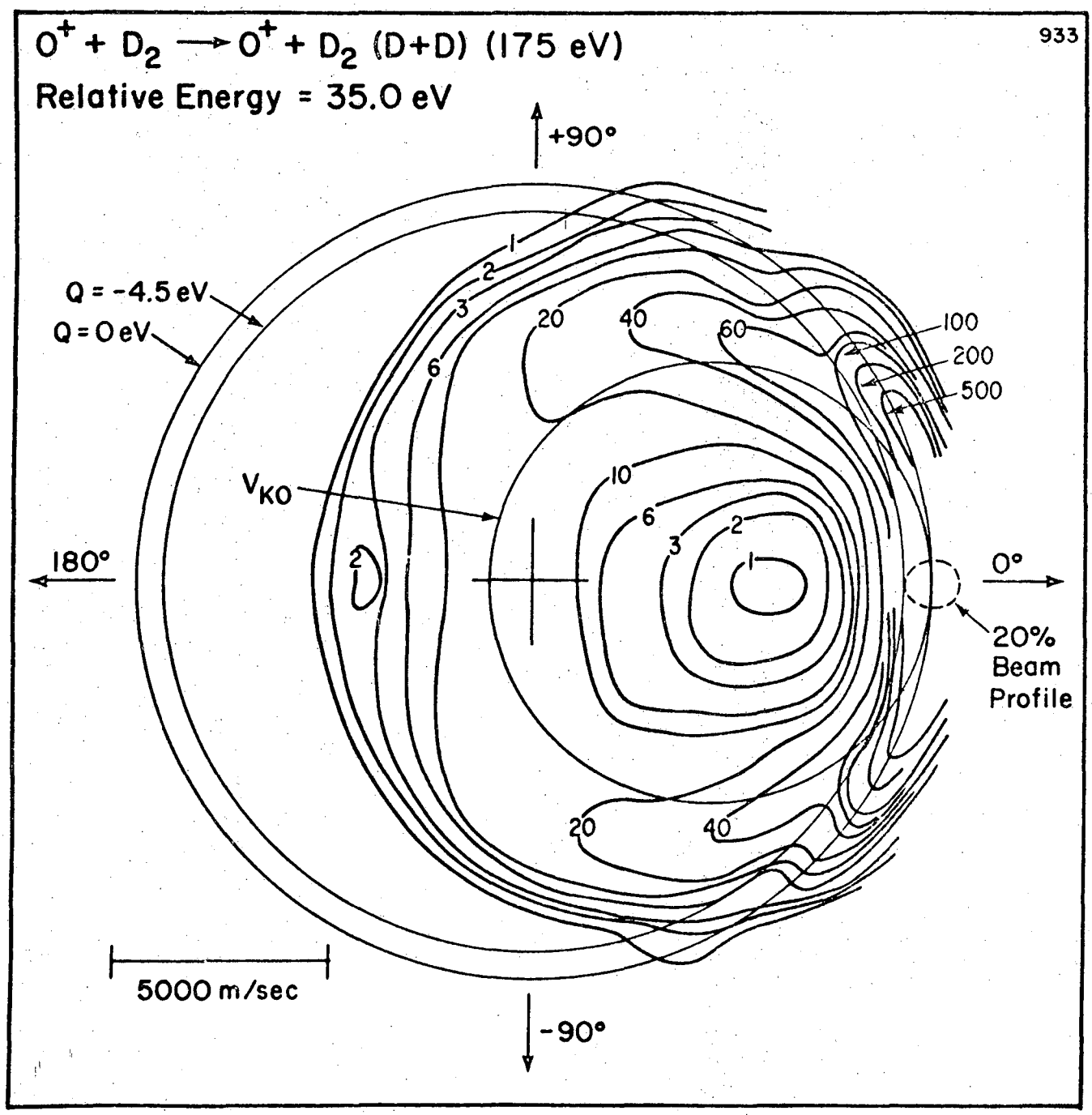

XBL 729-6915

Fig. 10

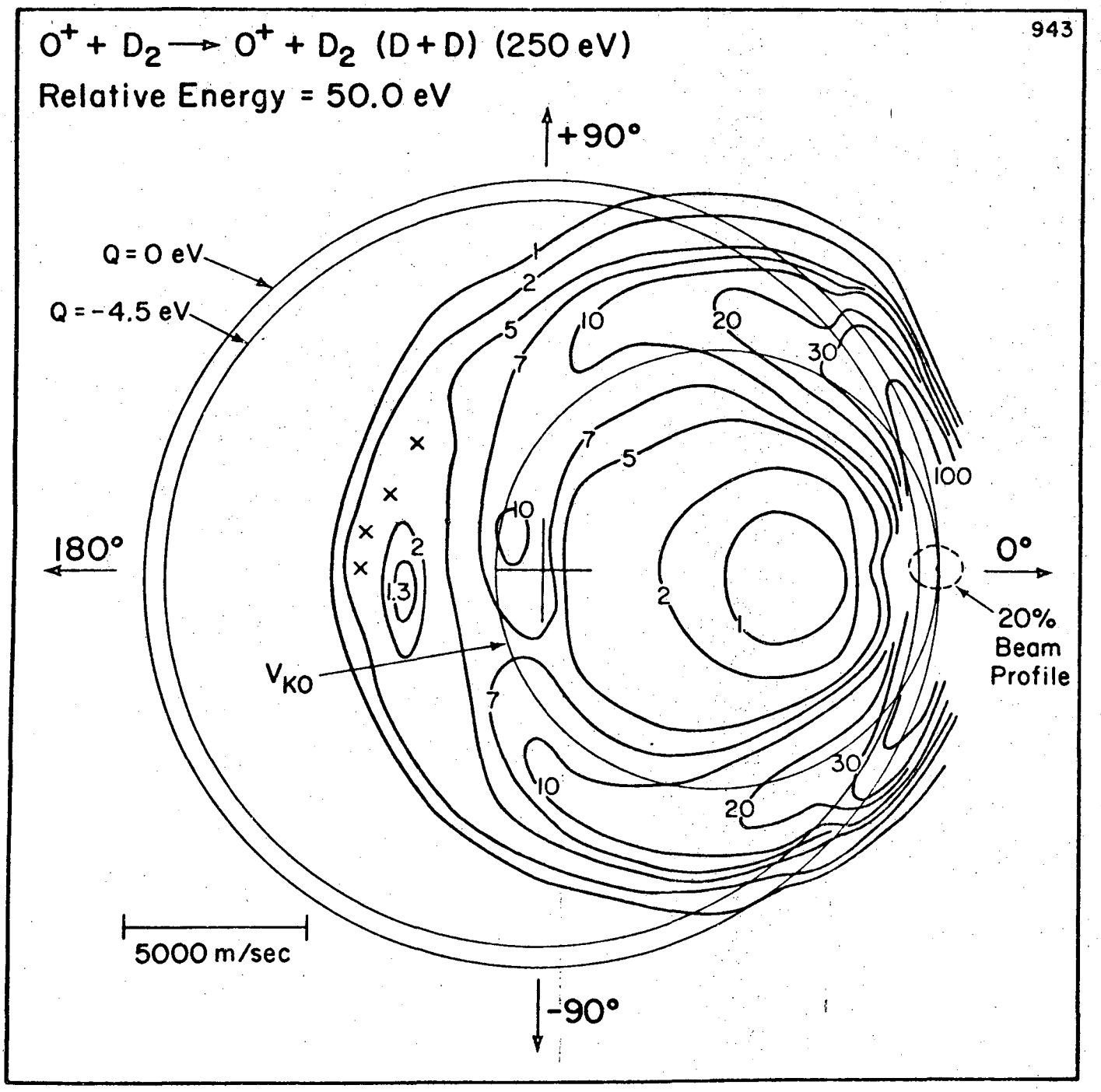

XBL 729-6910

Fig. 11

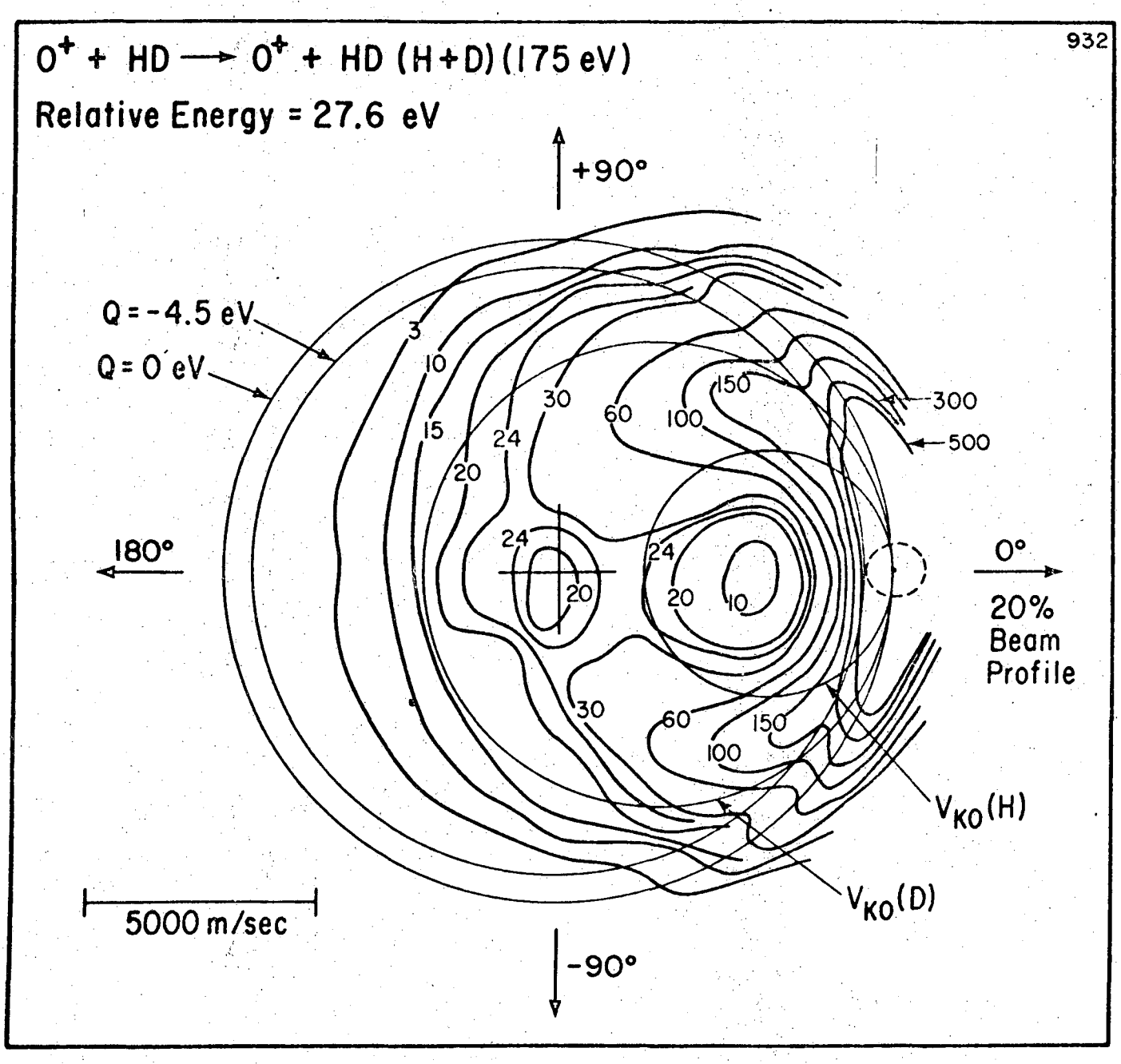

XBL729-6911

Fig. 12

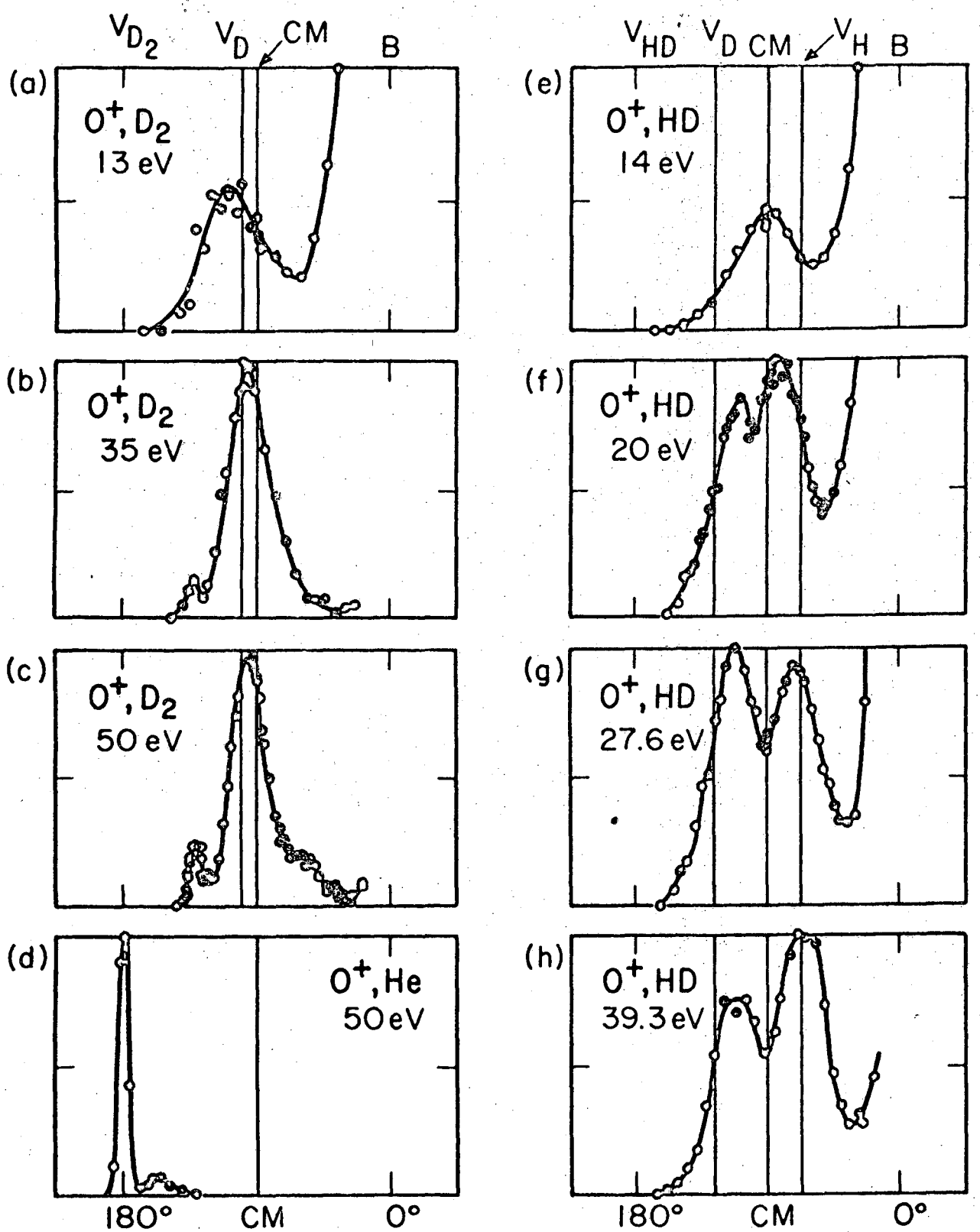

XBL 737-6519

Fig. 13

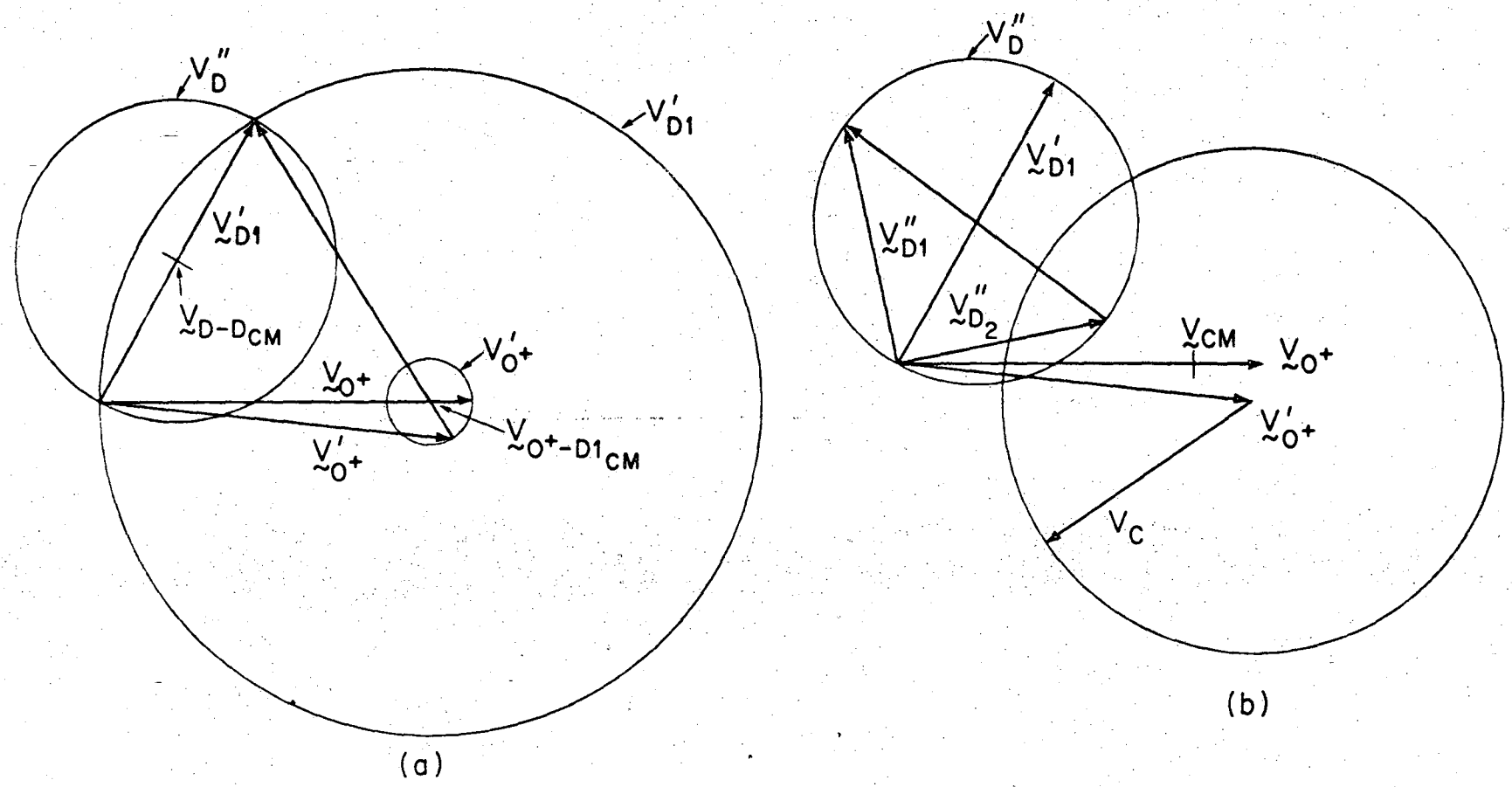

XBL 737-6516

Fig. 14

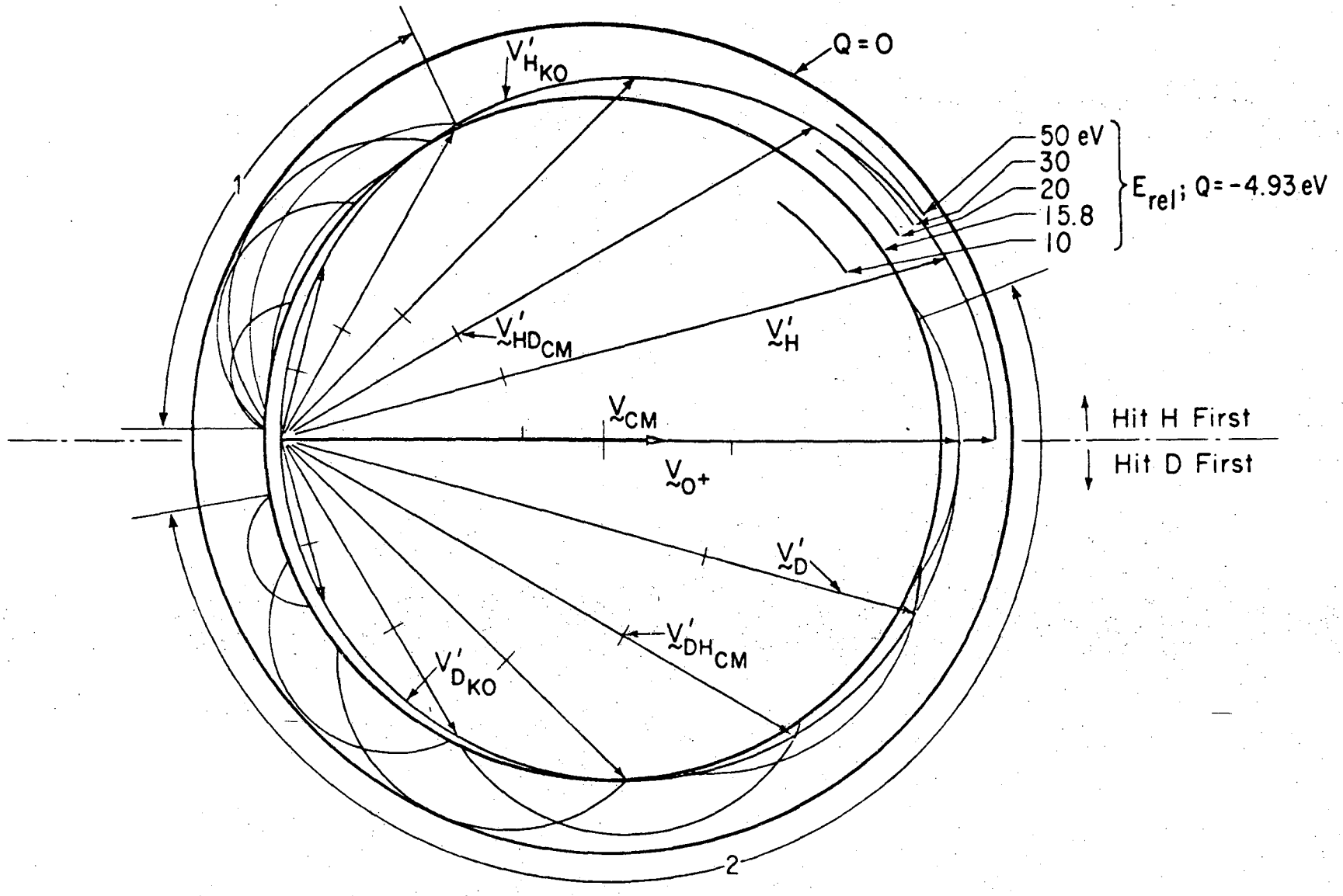

XBL 737-6517

Fig. 15

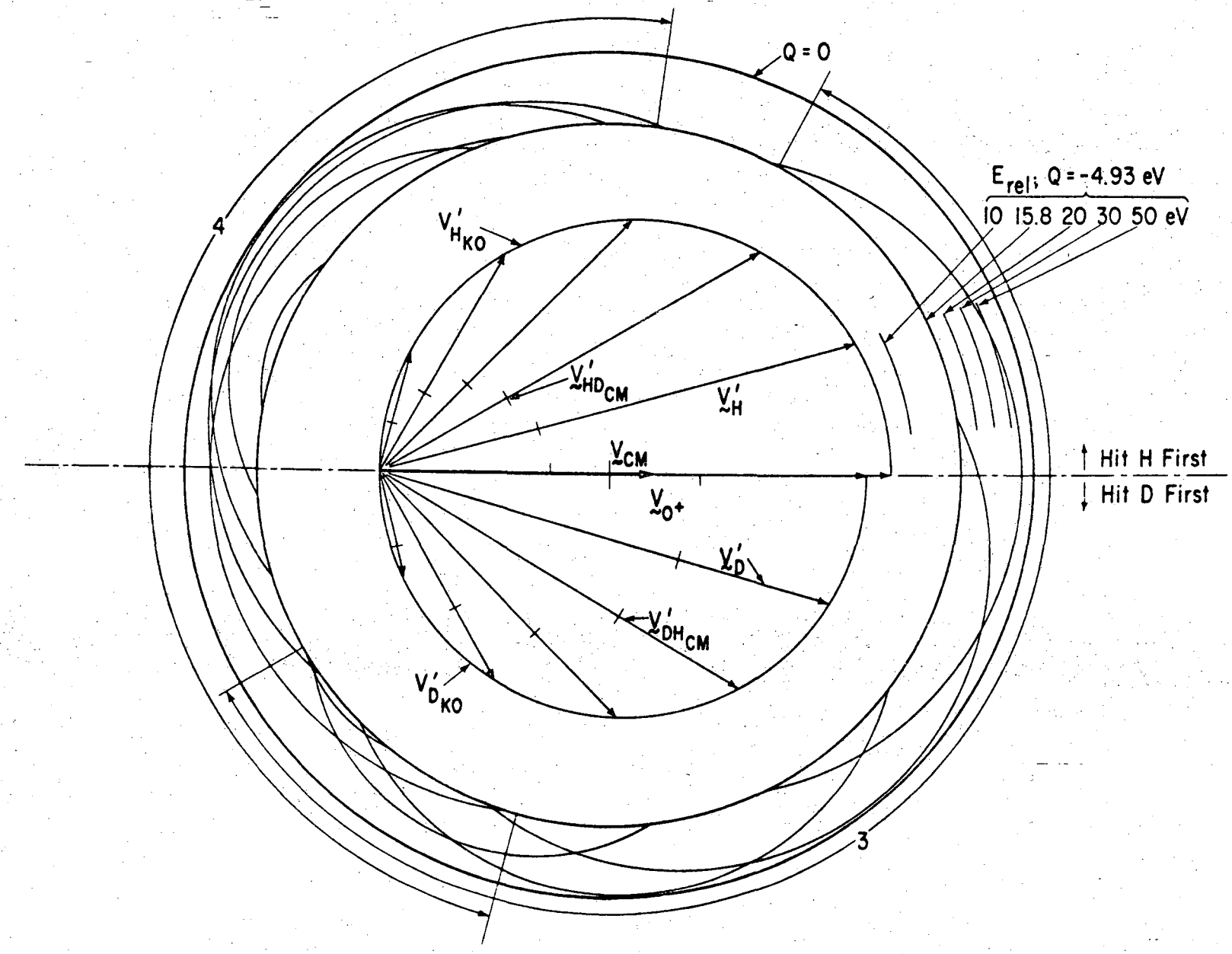

XBL 737-6518

Fig. 16

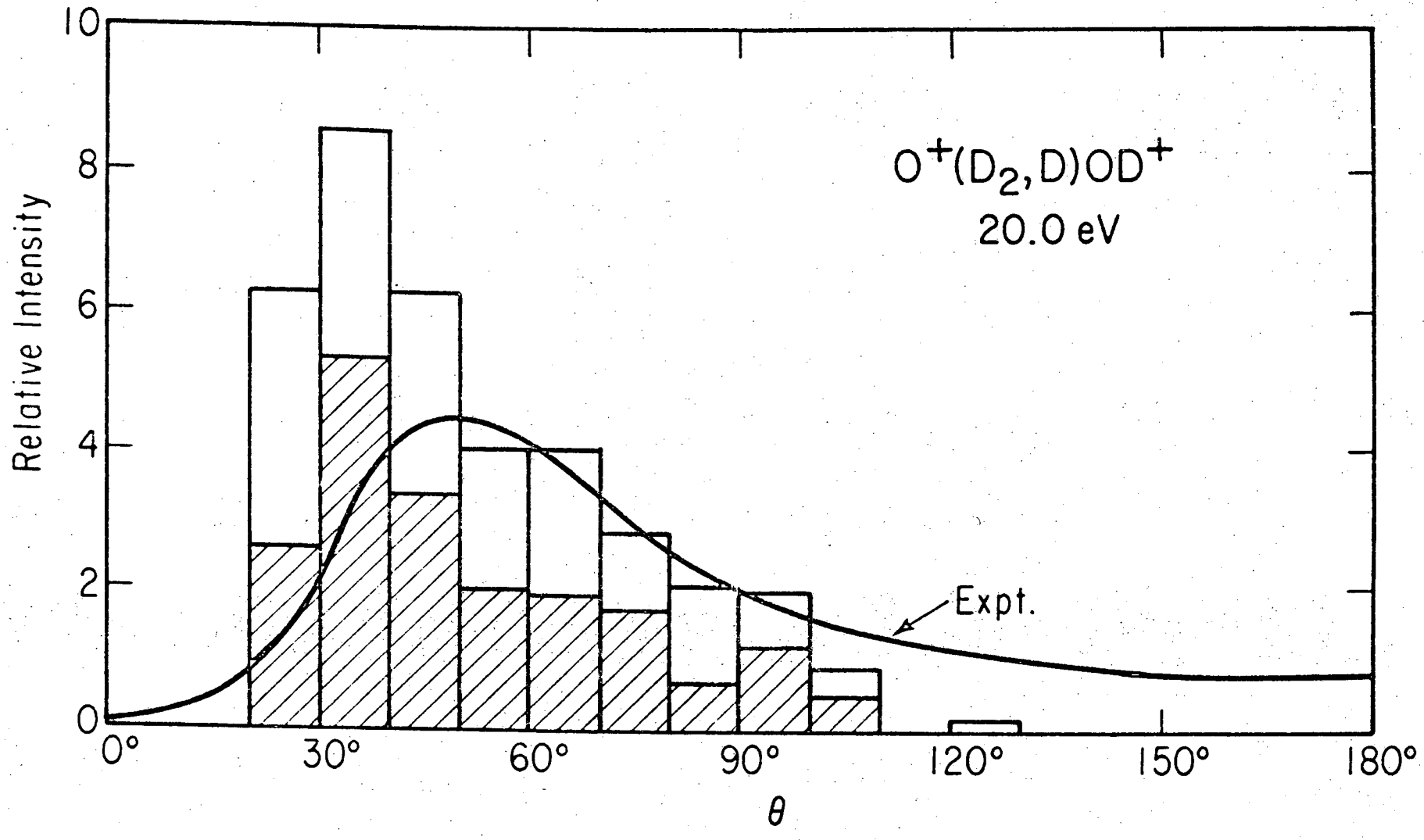

XBL 737-6515a

Fig. 17

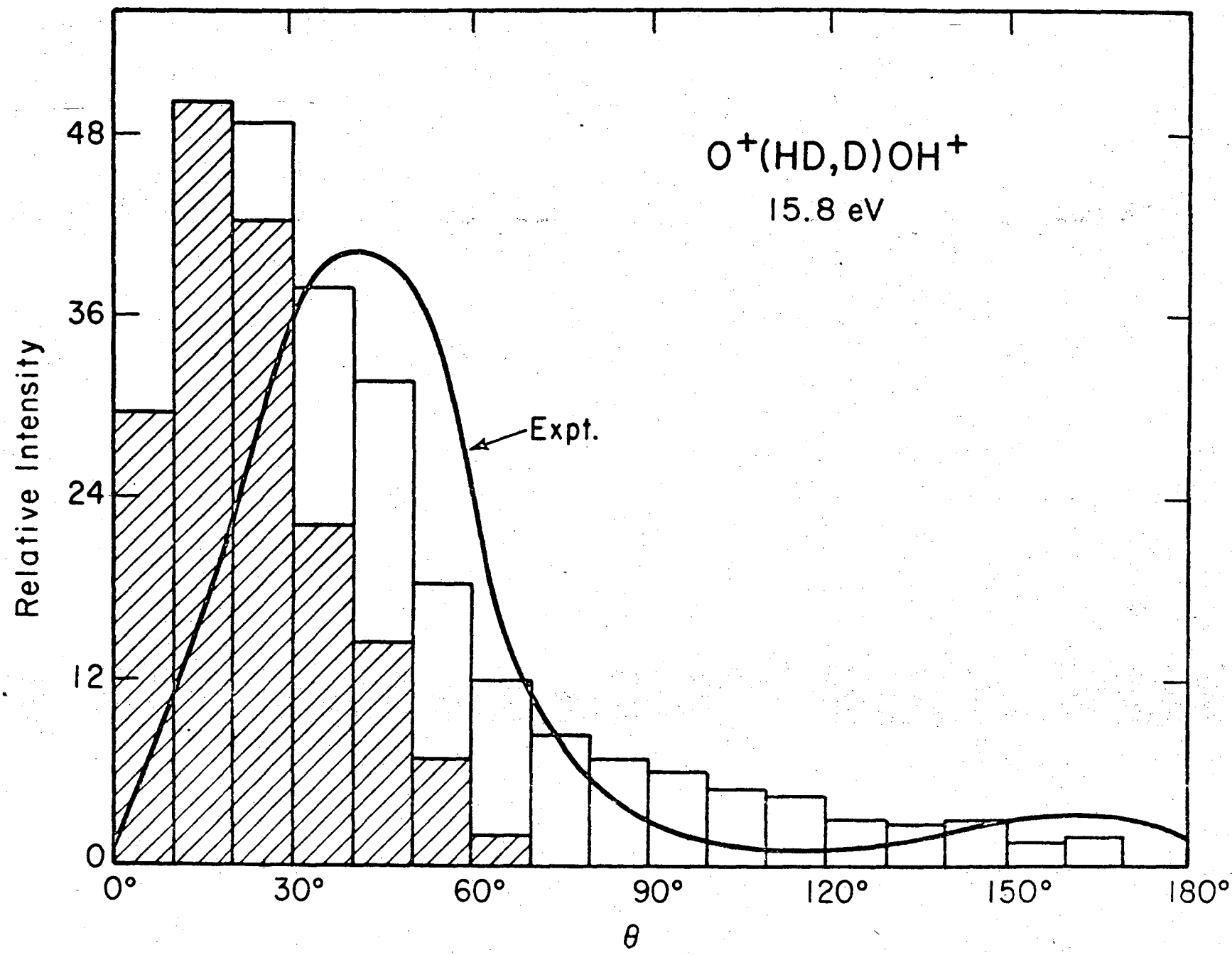

XBL 735-6132a

Fig. 18

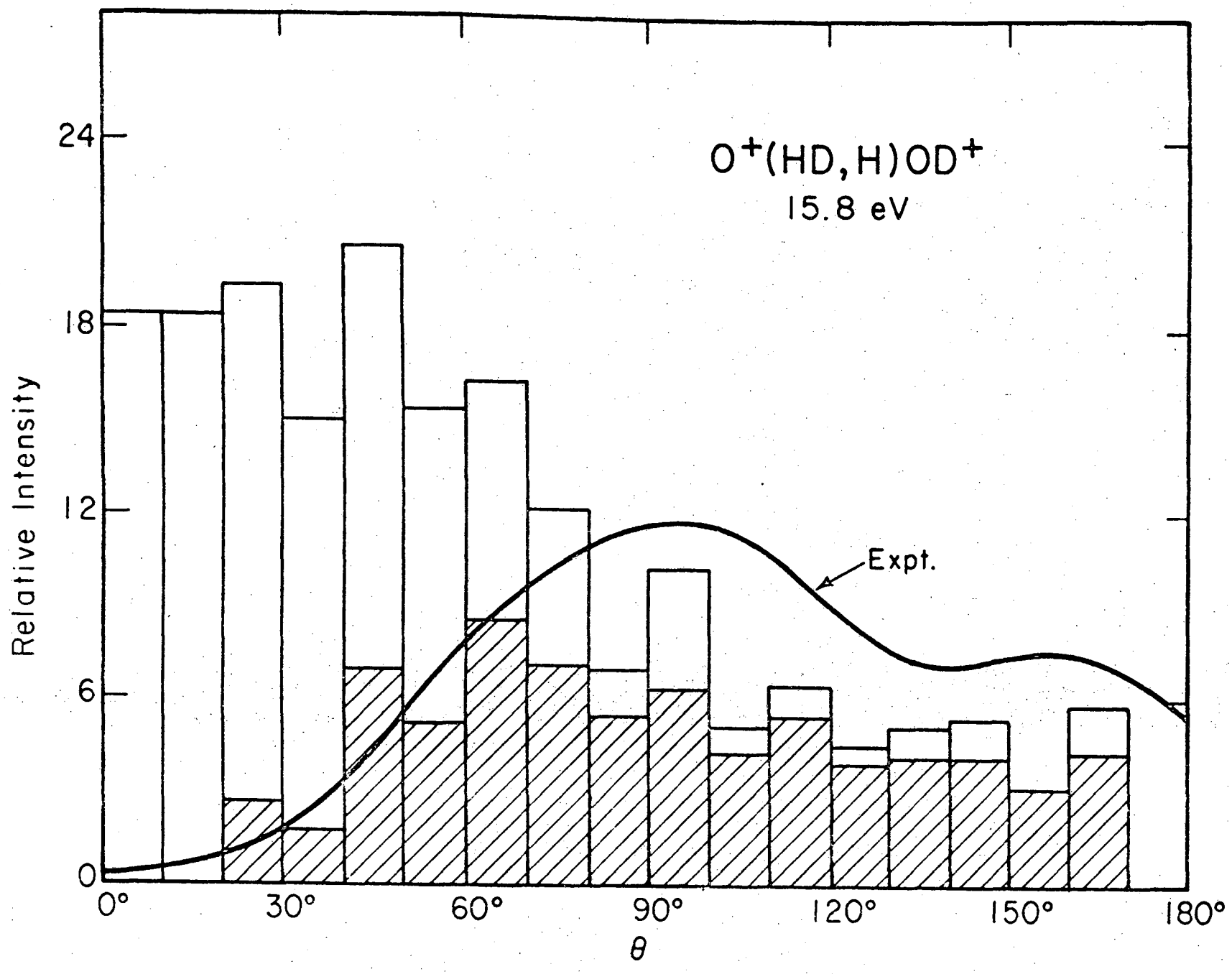

Fig. 19

XBL 735-6133a

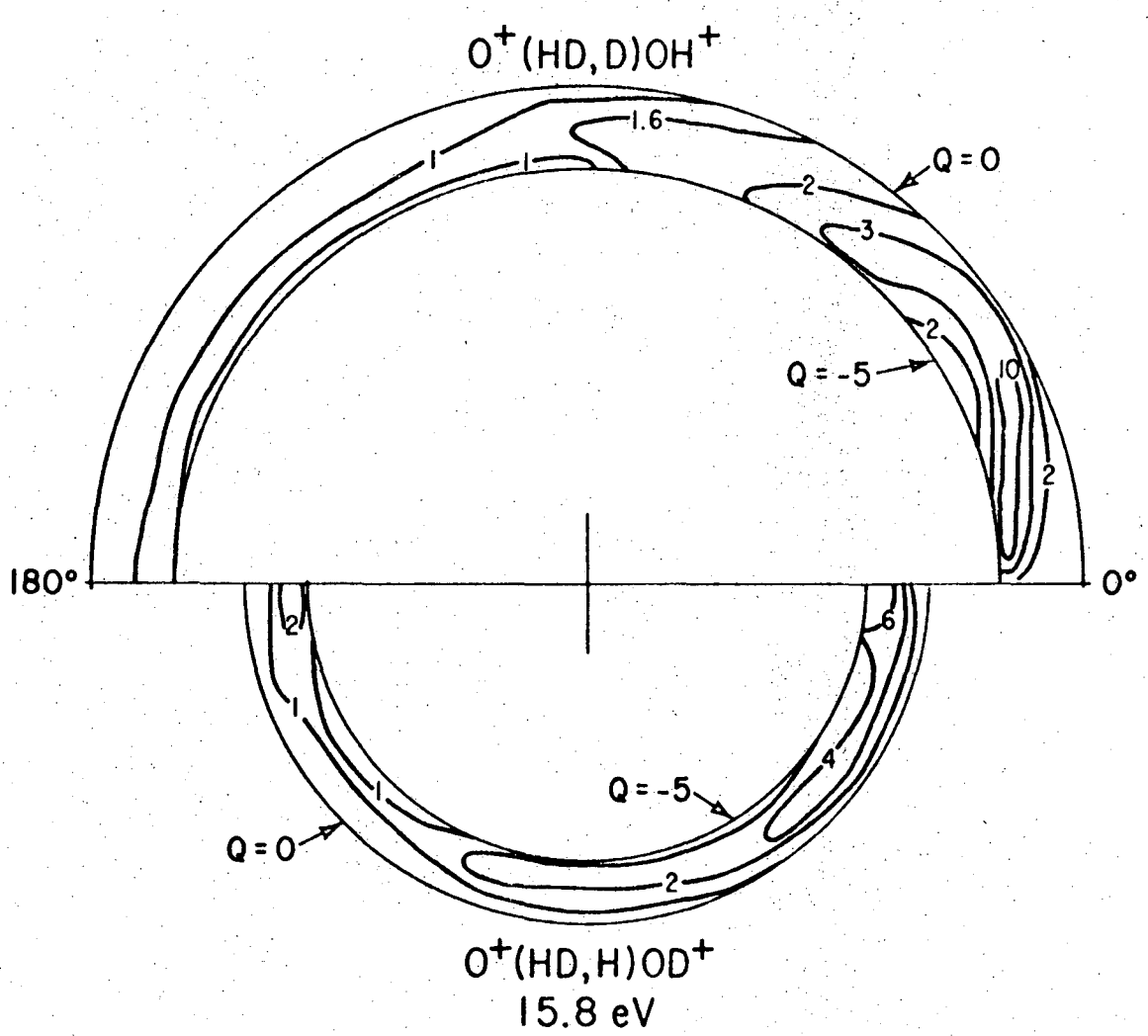

XBL 735-6128a

Fig. 20

LEGAL NOTICE

This report was prepared as an account of work sponsored by the United States Government. Neither the United States nor the United States Atomic Energy Commission, nor any of their employees, nor any of their contractors, subcontractors, or their employees, makes any warranty, express or implied, or assumes any legal liability or responsibility for the accuracy, completeness or usefulness of any information, apparatus, product or process disclosed, or represents that its use would not infringe privately owned rights.

TECHNICAL INFORMATION DIVISION
LAWRENCE BERKELEY LABORATORY
UNIVERSITY OF CALIFORNIA
BERKELEY, CALIFORNIA 94720